

# Possible Implications of a Vortex Gas Model and Self-Similarity for Tornadogenesis and Maintenance

DOUG DOKKEN, \* KURT SCHOLZ, AND MIKHAIL M. SHVARTSMAN

*Mathematics Department, University of St. Thomas, Saint Paul, MN*

PAVEL BĚLÍK

*Mathematics Department, Augsburg College, Minneapolis, MN*

COREY K. POTVIN

*Cooperative Institute for Mesoscale Studies, and NOAA/OAR/National Severe Storms Laboratory, Norman, OK, USA*

BRITTANY A. DAHL

*School of Meteorology, University of Oklahoma, Norman, OK, USA*

AMY MCGOVERN

*School of Computer Science, University of Oklahoma, Norman, OK, USA*

## ABSTRACT

We describe tornado genesis and maintenance using the 3-dimensional vortex gas model presented in Chorin (1994). High-energy vortices with negative temperature in the sense of Onsager (1949) play an important role in the model. We speculate that the formation of high-temperature vortices is related to the helicity inherited as they form or tilt into the vertical. We also exploit the notion of self-similarity to justify power laws derived from observations of weak and strong tornadoes presented in Cai (2005), Wurman and Gill (2000), and Wurman and Alexander (2005). Analysis of a Bryan Cloud Model (CM1) simulation of a tornadic supercell reveals scaling consistent with the observational studies.

## 1. Introduction

A recent paper (Cai 2005) defines the pseudovorticity by  $\zeta_{pv} = \frac{\Delta V}{L}$ , where  $\Delta V = |(V_r)_{\max} - (V_r)_{\min}|$  is the difference between the maximum and minimum radial velocity of the mesocyclone (rotating updraft) and  $L$  is the distance between them. Mobile Doppler radar observations of past tornadic and nontornadic storms were filtered using a range of Cressman influence radii (lower-bounded by the native data resolution and upper-bounded by mesocyclone diameter) to obtain points  $(\log(\varepsilon), \log(\zeta_{pv}))$ , where  $\varepsilon$  is the finest resolvable scale of the filtered radar data. Cai then calculated the regression line for each storm and found that steeper slopes (smaller negative values) are indicative of tornadic storms, and that the threshold for strong tornadoes in his sample was approximately  $m = -1.6$ . The regression lines Cai calculated strongly fit the data over scales between that of the mesocyclone core and that of the “edge” of the mesocyclonic tangential flow, indicating a vorticity vs. scale power law is valid over those scales. This suggests a power law for the decay of the vertical

component of vorticity outside the solid-body mesocyclone core of the form  $\zeta \propto r^b$ , where  $r$  is the radial distance from the axis of the vortex. Cai observed that it may be correct to interpret the exponent as a fractal dimension associated with the vortex. The vorticity power law, if valid, may extend to smaller (including tornadic) scales, but this could not be determined given the limited resolution of the radar observations used in Cai’s study.

In a paper devoted to analyzing mobile radar data obtained from a tornado that occurred in Dimmit, Texas (June 2, 1995) and was rated F2–F4, Wurman and Gill found  $v \propto r^b$ , i.e., the tangential winds outside the tornado core roughly fit the modified Rankine vortex model. (Wurman and Gill 2000). They calculated the exponent  $b$  and found it to vary from  $-0.5$  to  $-0.7$ . From data obtained in the intercept of the Spencer, South Dakota F4 tornado (May 31, 1998), Wurman and Alexander calculated  $b = -0.67$  (Wurman and Alexander 2005). Cai (Cai 2005) noticed that the (threshold) vorticity power law exponent for strongly tornadic mesocyclones in his sample

differs from the velocity power law exponent calculated for the strong tornado in (Wurman and Gill 2000) by 1, which is consistent with the vorticity being the curl of the velocity. The larger vorticity/velocity power law exponents found in strongly tornadic mesocyclones is consistent with the observation of (Trapp 1999) that “parcels that nearly conserve angular momentum penetrate closer to the central axis of the tornadic mesocyclones, resulting in large tangential velocities.” As noted by Cai, hurricanes exhibit a similar velocity power law and exponent outside their eyewall (e.g., Miller 1967). This suggests that roughly the same vorticity power law may apply over a range of atmospheric vortices.

Power laws with a particular scaling exponent arise when a phenomenon “repeats itself on changing scales” (Barenblatt 1996, 2003) see also (Barnsley 1988; Mandelbrot 1983). This property is called self-similarity. We propose that to more completely understand strong atmospheric vortices requires further exploration of their self-similarity. Self-similarity, especially when exhibited across objects ranging in scale, can point to important properties of the underlying dynamics. We focus on the possible self-similarity of tornadoes in this paper. As will be shown, tornadoes appear to exhibit local self-similarity and local homogeneity suggesting fractal phenomena.

The paper is organized as follows. In Section 2 we describe the tornadogenesis problem. In Section 3, motivated by the results of (Cai 2005; Wurman and Gill 2000; Wurman and Alexander 2005), we discuss a numerical experiment producing a time series of slopes of vorticity lines and its connection with previous results. In Section 4 we address self-similarity of tornadoes and mesocyclones and the way it might be manifested. We also give a heuristic argument supporting Cai’s power law and its associated exponent for strong tornadoes. In Section 5 we discuss the vortex gas theory of (Onsager 1949; Chorin 1994) in two and three dimensions and give arguments for its role in modeling tornadogenesis and tornado maintenance. In Section 6 we discuss suction vortices. In Section 7 we give conclusions and describe future work.

## 2. Tornadogenesis

The search to understand tornadogenesis invariably involves the question: “Where does the vorticity in the tornado originate?” The most penetrating studies of this question have led to the study of two types of vorticity: barotropic vorticity and baroclinic vorticity. Barotropic vorticity is vorticity that exists in the ambient environment and is frozen in the fluid and stretched and advected by the fluid. Baroclinic vorticity is vorticity that is generated by density currents in the fluid and is stretched and advected by the fluid. Definitive discussions of the role of barotropic and baroclinic vorticity in tornadogen-

esis and the mathematical decomposition of vorticity into barotropic and baroclinic parts and its consequences are given in (Davies-Jones 1984, 1982, 2000, 1996, 2006a,b, 2008). Both types of vorticity or combinations thereof have been suggested as the origins of the vorticity in tornadogenesis. Based on film footage of tornadoes showing sheets of precipitation spiraling into tornadoes, Fujita suggested a “barotropic” method called “Fujita’s recycling hypothesis” in (Fujita 1973, 1975). In this process the precipitation falling near the interface between the updraft and downdraft transported vorticity to the surface and into the tornado, and the precipitation-rich air was recycled into the thunderstorm updraft by the tornado. This hypothesis was explored in (Davies-Jones 2008; Markowski et al. 2003). The numerical model and experiment of (Davies-Jones 2008) shows that tornadogenesis can take place by a purely barotropic process. Numerical studies have also found that baroclinic vorticity can be important, if not dominant, in tornadogenesis in a recycling-type process as well (Markowski et al. 2003). Additional evidence supporting the recycling hypothesis is the observation that downdrafts associated with tornadic storms are generally warmer than downdrafts associated with storms that were nontornadic; this would make the updraft more buoyant in the tornado-producing storms and less buoyant in storms that do not produce tornadoes (Markowski et al. 2002).

Recent studies of radar data (Markowski et al. 2008) and numerical simulations (Straka et al. 2007) reveal arching vortex lines (or vortex tubes) in the rear flank of supercell storms. These vortex lines appear to be almost synonymous with supercell thunderstorms. If these vortex lines can be focused into a small region, as more and more vortex lines enter this region, viscous interactions between neighboring vortex lines are believed to lead to mergers. This can ultimately lead to the creation of a strong vortex. Several theories have been given for the production of the arching vortex lines. In one theory (Markowski et al. 2008; Straka et al. 2007) vorticity lines (or rings) baroclinically generated around the rear flank downdraft are advected toward the updraft as they descend. The downstream portions of the vorticity lines are subsequently lifted and stretched by the updraft while the upstream portions continue to descend, forming vortex arches. A second theory holds that horizontal shear across the rear flank gust front is the source of the vortex arches (Lee and Wilhelmson 1997a,b, 2000; Trevorrow et al. 2012). This would create a vortex sheet that could be stretched and rolled up into a tornado vortex. It seems plausible that a combination of these two processes could be present, with a reconnection of vortex lines produced by the two different processes. However, there may be other vorticity sources as well. As discussed later, we hypothesize that the possible fractal dimension of 1.6 found in (Cai 2005) and implied in Wurman’s observational studies comes from the interactions of

vortices produced in these shear regions.

Observational analysis of videos of the tornadogenesis phase in large-diameter tornadoes forming under low-cloud bases (see, e.g., (Discovery.com/stormchasers 2010)) suggests that vortices (vortex lines) which enter the developing tornado make a partial revolution about the ambient tornado vortex before folding up and dissipating. The vortex gas theory developed in Section 5 suggests this folding up is necessary to conserve energy as the vortex stretches and/or interacts with other vortices (Chorin 1994). In this process some energy is transmitted to much smaller scales, the so-called inertial range, beginning the Kolmogorov cascade to the viscous range and then dissipating as heat. However, before kinking up, as the vortex stretches much energy is transmitted to the ambient vortex as kinetic energy of the flow and this increases the vorticity of the tornado. In this theory, as more and more vortices successively enter the developing tornado, the process repeats itself many times gradually increasing the vorticity of the tornado vortex. Subsequently, the vorticity of the ambient vortex is increased (assuming the vortex lines are produced uniformly), which can be further enhanced by stretching, eventually achieving quasi-equilibrium with its environment. During this process, energy is transferred from the smaller scales to the larger scales in an inverse energy cascade. As more vortices enter the ambient tornado vortex, larger vortices tend to form; the stronger vortices at the core and slightly weaker vortices wrapping around them. Visually, the resulting flow could manifest itself as multiple vortices or as a large single vortex. The stretching of the vortices that enter the tornado eventually leads to the dissipation of their vorticity in a Kolmogorov cascade. The process just described contrasts with the transition to a multiple-vortex configuration that can occur when the critical swirl ratio (a measure of tornado-scale helicity) is exceeded (e.g., (Church et al. 1977)).

It has been shown (Moffat 1969; Moffat and Tsinober 1992) that twisting of subvortices about one another is measured by the helicity of the parent vortex. Helicity is the integral over physical space of the dot product of the velocity and the vorticity. It is thought that helicity of a flow inhibits the dissipation of energy and helps maintain the intensity of the flow (Levich and Tzvetkov 1985; Lilly 1983, 1986a,b). The use of helicity as a tool in studying supercell thunderstorms was initiated by (Lilly 1983, 1986b) and (Davies-Jones 1984; Davies-Jones et al. 1990). It has been used in a slightly modified form as a parameter to study its effect on supercell storms (Davies-Jones 1984; Davies-Jones et al. 1990; Droegemeier et al. 1993). Lilly thought of a vortex as a coiled spring that unwinds as it stretches (Lilly 1983, 1986b). If we think of the helicity as measuring how much the vortex is wound up, the stretching unwinds the spring and releases energy to the surrounding flow. This unwinding could manifest itself as

vortex breakdown and/or the fractalization and kinking up that is predicted in the vortex gas theory (described later).

A series of papers (Lee and Wilhelmson 1997a,b, 2000) studied non-supercell tornadogenesis due to vertical shear in the boundary layer. They considered a weak cold pool (outflow boundary) advancing from the west into an ambient flow from the south to the north. This led to a south-to-north oriented vortex sheet forming at the interface of the two flows. They noted first-generation vortices rolling up into stronger second-generation vortices. It seems plausible that if one did finer-grid simulations of the situation considered in (Lee and Wilhelmson 1997a,b, 2000), the first-generation vortices would have formed from roll-ups at smaller scales, etc., resulting in a self-similar structure. The structure of the resulting vortex sheet resembled that of (Baker and Shelley 1990). The roll-up process has also been studied by (Rotunno 1984; Snow 1978). Snow concludes that “the subsidiary vortices are integral parts of the overall flow pattern and should not be viewed as interacting independent vortices.” Once vortex sheet roll-up has occurred, tornadogenesis can be induced by convection moving over and stretching one of the vortex sheet vortices. The first of three non-supercell tornadoes studied by (Roberts and Wilson 1995) formed in this manner.

With sufficient stretching, non-supercell tornado vortices have achieved EF3 strength (Roberts and Wilson 1995), but virtually all violent (EF4-EF5) tornadoes occur within supercells. While this suggests important differences between tornadogenesis mechanisms in supercells versus non-supercells, it does not preclude the possibility that vortex sheet roll-up can also play an important role in supercell tornadogenesis. Radar (Bluestein et al. 2000, 2003b; Bluestein and Pazmany 2000; Bluestein et al. 2003a; Dowell and Bluestein 1997, 2002a,b) and observational (Brandes 1978; Wakimoto and Wilson 1989; Wakimoto and Atkins 1996; Wilson 1986) analyses have revealed vortices along the rear flank gust front of both tornadic and nontornadic supercell storms. The role of these vortices in tornado formation is a subject of current research. As with non-supercells, supercell tornadogenesis has been observed to sometimes be triggered when one of these vortices is stretched by an updraft (Wakimoto and Atkins 1996) (but this process alone probably cannot produce violent tornadoes). Consistent with observations, numerical supercell simulations have shown vortices that appear to form along the edge of the rear flank gust front or a secondary gust front then roll up into a tornado vortex (Adlerman and Droegemeier 2000). The resulting vorticity distribution at one stage of tornadogenesis in (Adlerman and Droegemeier 2000) resembles the two-dimensional vortex sheet roll-up modeled by (Chorin and Bernard 1973) and Krasny (Krasny 1993). The remarkable photo taken by Gene Moore (see Figure 1) strongly implies vortex sheet roll-up. A sequence of vortices appears to be spiraling into a tornado as it crosses

a lake. These feeder vortices have cross-sections too small to be resolved in all but the highest-resolution simulations currently achievable and appear to be very intense. Evidence of similar feeder vortices is also shown in Figure 2, in which tracks left in corn fields appear to show vortices spiraling into the tornadoes and then dissipating as they stretch.

Subsequent to vortex sheet roll-up, vortex mergers may play a critical role. Observations of tornadogenesis near Bassett, NE (Bluestein et al. 2000) suggested that a larger vortex ( $\sim 500$  m scale) and a smaller vortex ( $\sim 100$ – $200$  m scale), both of which were conjectured to arise from vortex sheet roll-up along the rear flank gust front, interacted such that the smaller vortex was absorbed by the larger vortex, possibly triggering tornadogenesis. The authors suggested that the origin of the vorticity was tilting of stream-wise vorticity along the rear flank gust front (Dowell and Bluestein 2002b). Tilting of stream-wise vorticity would result in vortices that have large helicity and are more resistant to dissipation due to stretching. In such a scenario, it is plausible that stretching and subsequent intensification of a larger vortex could draw other vortices through their mutual interaction, resulting in vortex mergers that further intensify the dominant vortex, and so on to tornadogenesis.

Further evidence that vortex sheet roll-up contributes to tornadogenesis in supercells is provided by (Chorin and Bernard 1973), which showed that vortex sheets consisting of cyclonically rotating vortices roll up into a cyclonic vortex. The rolled up vortex sheet resembled the hook echo region of a supercell thunderstorm. We believe the roll-up in (Chorin and Bernard 1973) is representative of the roll-up in (Adlerman and Droegemeier 2002). When vortices of opposite sign were placed in the two halves of the vortex sheet segment, the sheet rolled up into a cyclonic, anticyclonic couplet resembling that often observed to straddle the hook echo and recently associated with arching vortex lines.

The process of tornadogenesis by roll-up of a vortex sheet undergoing stretching by the mesocyclone updraft occurs in the numerical simulation described in Section 3 and is illustrated in Figure 3. The time series for the maximum surface vorticity within the developing tornado can be found in Figure 8. Note how the vortex sheet vortices intensify as they stretch and approach the developing tornado. As the vortex sheet rolls up the vortices transfer energy to the developing tornado vortex, increasing its maximum vorticity from  $\sim 0.1$   $s^{-1}$  to  $\sim 0.7$   $s^{-1}$  over the 3-minute period shown. In Figure 4, taken from (Wurman et al. 2013), maximum gate-to-gate shear in an observed tornado exhibits marked oscillations superimposed on an upward trend. Given that the tornado did not display multiple-vortex behavior, we speculate that the shear oscillations and gradual increase in kinetic energy resulted from ab-

sorption of successive vortex sheet vortices, similar to that in the simulation. As such vortices are absorbed they would contribute not only energy but also helicity, which would decrease energy dissipation in the tornado (Lilly 1986a,b; Yokoi and Yoshizawa 1993; Andre and Lesieur 1977).

### 3. Vorticity lines computed from numerical simulation

A supercell thunderstorm simulation was investigated to help confirm the conclusions of (Cai 2005) regarding the evolution of mesocyclone vorticity lines prior to and proceeding tornadogenesis. The supercell was simulated using the compressible mode of the non-hydrostatic Bryan Cloud Model 1 (CM1; (Bryan and Fritsch 2002)). The simulation proceeded on a  $112.5$  km  $\times$   $112.5$  km  $\times$   $20.0$  km domain with horizontal grid spacing of  $75$  m and vertical grid spacing increasing from  $50$  m at the lowest layer to  $750$  m at the highest layer. The large and small time steps were  $1/4$  s and  $1/16$  s, respectively. Typical of idealized storm simulations, a horizontally uniform analytical base state was used (see Figure 5), terrain, surface fluxes, radiative transfer, and Coriolis acceleration were omitted, and radiative (free slip) lateral (vertical) boundary conditions were imposed. Microphysical processes were parametrized using the double-moment (Morrison et al. 2005) scheme. The subgrid turbulence scheme was similar to (Deardorff 1980). The simulated supercell exhibits features commonly observed in real supercells, including a hook echo reflectivity signature with a cyclonic–anticyclonic vorticity couplet (see Figure 6).

To compute maximum vorticity at different length scales  $\varepsilon$ , the vorticity field valid on the  $75$ -m simulation grid was filtered using the Cressman interpolation method (Cressman 1959) with the cutoff radius set to  $2\varepsilon$  (consistent with (Cai 2005)). Vorticity lines were then computed near the low-level mesocyclone  $\sim 500$  m above ground level (AGL) every 5 minutes once a distinct low-level mesocyclone had formed (as discerned from visual inspect of the  $75$ -m vorticity field). As in (Cai 2005), vorticity lines were fit to  $300$  m  $\leq \varepsilon \leq 9600$  m. Tornadogenesis was considered to occur once the maximum axisymmetric tangential wind velocity,  $V_T$ , around the intensifying surface vortex associated with the low-level mesocyclone exceeded  $20$  m  $s^{-1}$ . The  $V_T$  was retrieved using the vortex detection and characterization technique of (Potvin 2013).

As in (Cai 2005), the vorticity lines steepen prior to tornadogenesis (see Figures 7 and 8), consistent with the concentration of vorticity from larger to smaller scales. Also as in (Cai 2005), a power law for vorticity appears to hold for scales exceeding that of the low-level mesocyclone core, but breaks down at smaller scales. (Cai 2005) attributed this to smaller scales being more poorly resolved in his radar dataset. A similar effect occurs in our scenario: the

Figure 1: ©Gene Moore, Vortex sheet roll-up.

effective model resolution (Frehlich and Sharman 2012) artificially decreases the energy contained at scales approaching the grid spacing. In the absence of positive evidence that the vorticity power law indeed extends to tornadic and smaller scales, we can only offer this as a speculative explanation for the flattening of the vorticity lines at sub-mesocyclone scales. As discussed later, however, Cai’s vorticity power law hypothesis (including its validity at tornadic scales) finds support in heuristic considerations of Kelvin-Helmholtz instability in vortex sheets.

#### 4. Self-Similarity

In this section we give possible ways mesocyclones and tornadoes might acquire self-similarity and so give rise to the hypothesized vorticity and velocity power laws discussed above.

Self-similarity can manifest itself in several ways in atmospheric flows. One such manifestation is scale-invariance of some characteristic of the flow, which may be demonstrated by the existence of a power law for the characteristic. Examples include the scenarios discussed above, where a power law for pseudovorticity (Cai 2005) or velocity (Wurman and Gill 2000; Wurman and Alexander 2005) are hypothesized.

Another manifestation is a geometric self-similarity, where features having similar shape occur at different scales. For example, (Church et al. 1977) illustrate a hierarchy of known vortex scales in tornadic supercells (see Figure 9). Figure 9 is strikingly similar to images on page 168 of (Arnold and Khesin 1999) and the Smale attractor cross-section on page 533 of (Katok and Hasselblatt 1995).

Geometric self-similarity is occasionally seen in Doppler radar and reflectivity observations (Bluestein and Pazmany 2000; Nova 2004) and high-resolution numerical simulations of tornadic supercells ((Nova 2004) and (Adlerman and Droegemeier 2000), see also Figure 10. High-quality video recordings of some recent tornadoes depict mini-suction vortices (subvortices of suction vortices), confirming the smallest scale of the hierarchy of (Church et al. 1977).

In a related work, (Bélik et al. 2014), some of the authors revisit Serrin’s “swirling vortex” model (Serrin 1972) and investigate solutions to the Navier–Stokes and Euler

equations in spherical coordinates with  $v \propto r^b$ , where  $b$  is not necessarily equal to  $-1$ . The streamlines of the modeled vortices exhibit self-similarity, i.e., both the power law and the geometric manifestations of self-similarity are addressed in this work.

Chorin in his study of turbulent flow found quantities with fractal dimension. In numerical experiments he found the fractal dimensions of the axes of vortices he studied to be related to the “temperature” of the vortex. “Hot” negative-temperature vortices had a smooth axis, while at temperatures of positive or negative infinity (Kolmogorov cascade) the vortex had a fractal axis (and cross section). We hypothesize that high-energy vortices entering the tornado acquire fractal axes upon being stretched and kinked up (transition from negative-temperature vortices to infinite-temperature vortices). One would expect a mixture of fractal dimensions for these axes in the turbulent region surrounding the solid body tornado core.

In their study of the effect of rotation and helicity on self-similarity, Pouquet and Mininni (2010) comment that “when comparing numerical simulations, it was found that two runs at similar Rossby number and at similar times (albeit at different Reynolds number) display self-similar behaviour or decreased intermittency depending on whether the flow had helicity or not.” That tornadoes form in helical environments may largely account for the degree of self-similarity that is often observed in them (e.g., presence of suction vortices), and suggests self-similarity may extend to smaller scales than currently known. We propose that such self-similarity can arise within persistent vortex sheets along the rear flank downdraft gust fronts of tornadic supercells. In the proposed scenario, a sequence of vortex roll-ups occurs, with each new generation of vortices forming from previous-generation vortices wrapping around each other, ultimately resulting in vortices with roughly fractal cross-sections (geometric self-similarity).

We now give a heuristic argument to support Cai’s power law for the vertical vorticity of strong tornadoes, i.e.,  $\zeta = \mathcal{O}(\epsilon^{\sim(-1.6)})$ . From Kelvin’s circulation theorem, the product of vorticity  $\zeta$  and the cross-sectional area of a vortex tube is constant for Eulerian barotropic flows. Hence,  $\zeta = C/A$ , where  $A$  is the cross-sectional area of the vor-

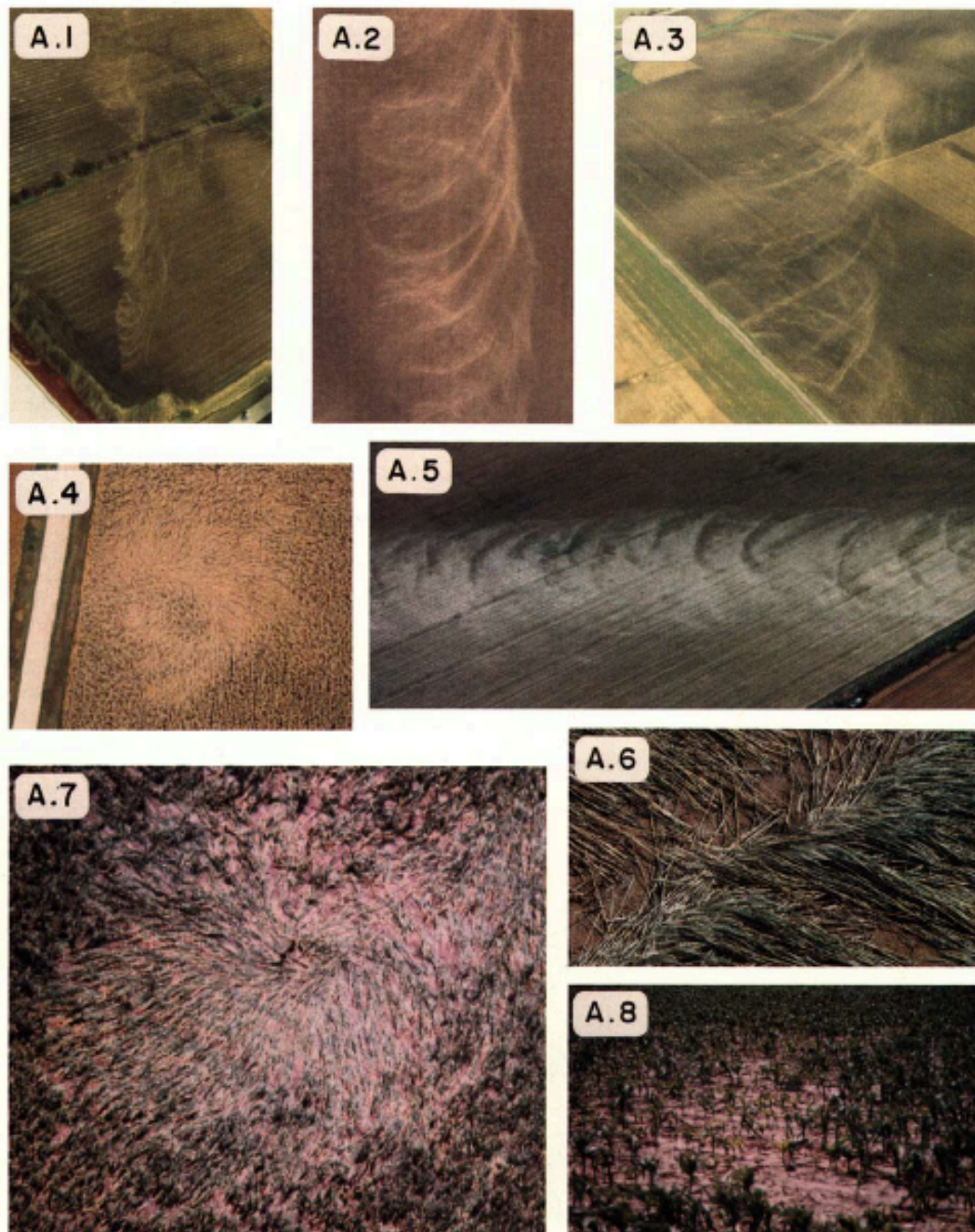


FIG. 14. Examples of ground marks left behind by suction vortices embedded inside tornadoes. Locations and dates of occurrences are: (A.1) Decatur, Illinois tornado 3 April 1974; (A.2) Magnet, Nebraska tornado, 6 May 1975; (A.3) Homer Lake, Indiana tornado, 3 April 1974; (A.4) Dubuque, Iowa tornado, 28 September 1972; (A.5) and (A.6) Pearsall, Texas tornado, 15 April 1973; (A.7) Mattoon Lake, Illinois tornado, 21 August 1977; (A.8) Grand Island, Nebraska tornado, 3 June 1980.

Figure 2: ©American Meteorological Society, Tornadoes and downbursts in the context of generalized planetary scales. *J. Atmos. Sci.*, **38**, 1511–1534.

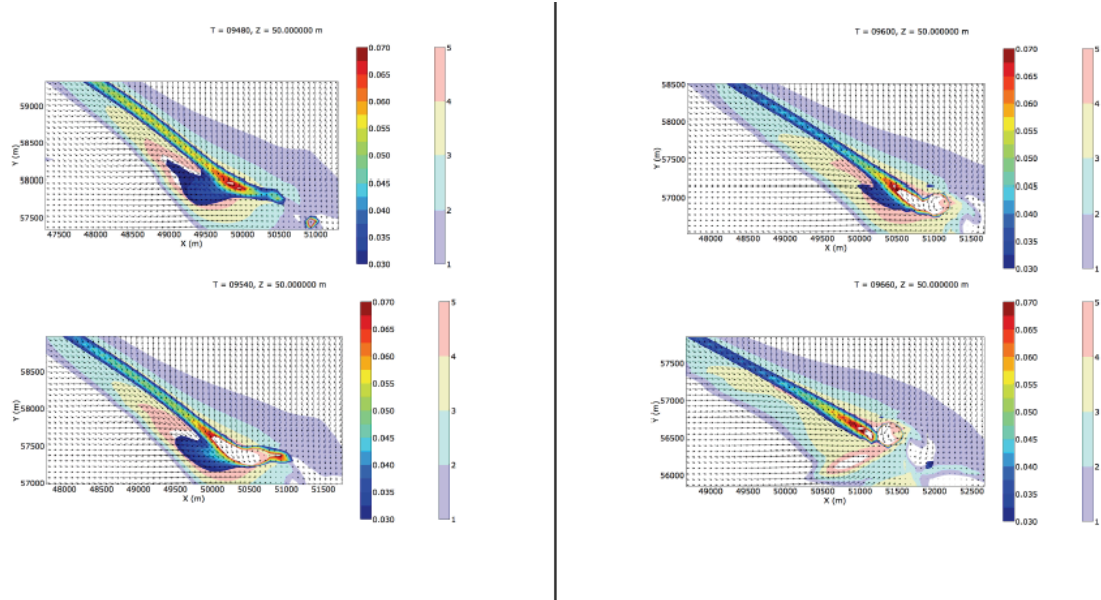


Figure 3: Vortex sheet roll-up in CM1 simulation at  $t = 9480$ ,  $t = 9540$ ,  $t = 9600$  and  $t = 9660$ ;  $z = 50$  m. The faded color shading is vertical velocity ( $\text{m s}^{-1}$ ). The darker color shading is vertical vorticity ( $\text{s}^{-1}$ ).

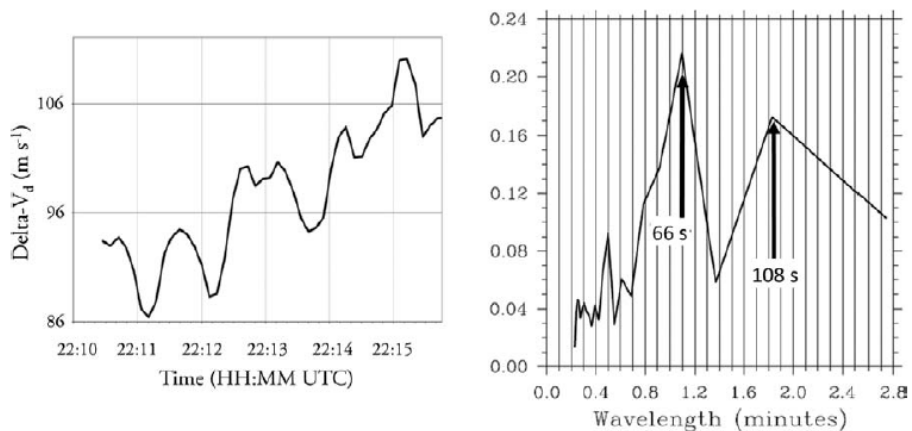


FIG. 7. (left) Oscillation of tornado intensity defined by maximum  $\Delta V = V_d$  (outbound)  $- V_d$  (inbound). (right) FFT of  $\Delta V$  with peak energy at 66 and 108 s, suggestive of rotating asymmetry in vortex.

Figure 4: ©American Meteorological Society, Time series of maximum gate-to-gate shear consistent with energy being pumped into the tornado in discrete pulses. Possibly from roll-up vortices within a vortex sheet.

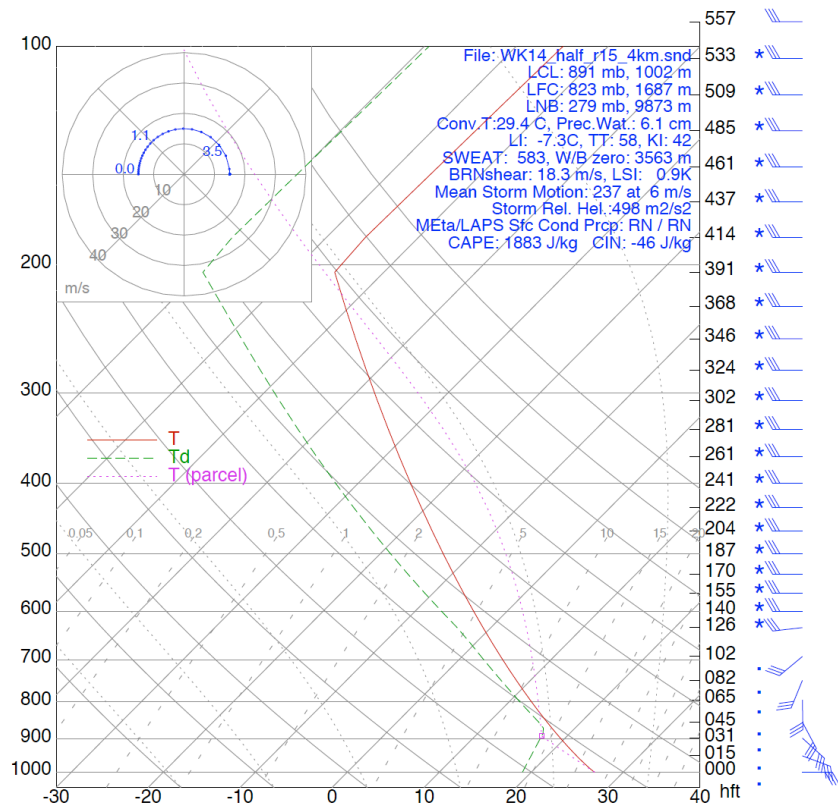


Figure 5: Base state for CM1 simulation. Wind barbs are in knots. The hodograph (upper left corner) is in  $\text{m s}^{-1}$ , with marked heights in km.

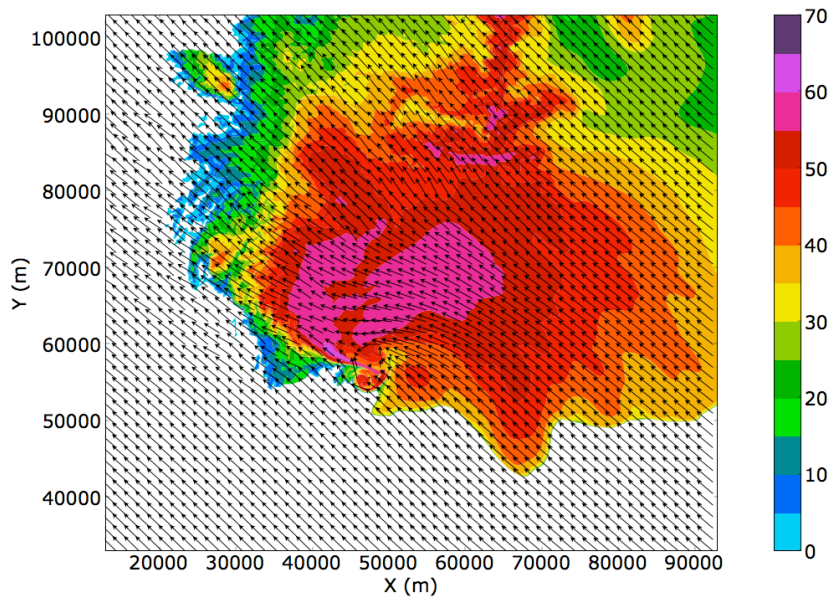


Figure 6: Simulated reflectivity field (dBZ) and horizontal wind vectors (arrows) valid  $\sim 0.5$  km AGL at  $t = 164$  min, near the time of tornadogenesis.



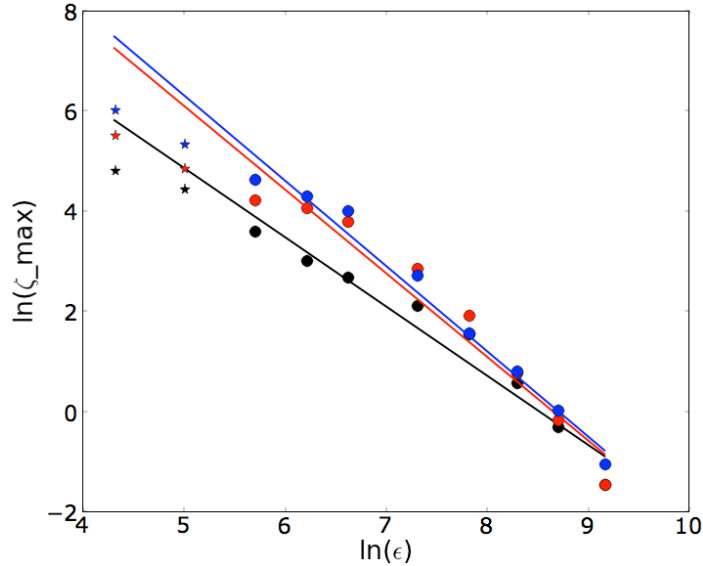


Figure 7: Vorticity lines computed at  $t = 134$  min (black), prior to the development of a discernible surface vortex; at  $t = 154$  min (red), by which time a relatively weak surface vortex is present; and at  $t = 169$  min (blue), near the time of tornadogenesis. Points used to create the least-squares fit are denoted by dots, while points not used in the vorticity line computation ( $\varepsilon < 300$  m) are denoted by asterisks.

tex. A numerical study of Kelvin–Helmholtz instability by (Baker and Shelley 1990) identifies a relationship between the thickness of the vortex sheet,  $h$ , and the cross-sectional area of the vortices,  $A$ . The result is that  $A$  scales like  $\mathcal{O}(h^{1.55})$  as  $h \rightarrow 0$ . To the degree that a tornado is formed from vortex sheet vortices, and that the hypothesized vorticity power law (and self-similarity) extends to tornadic and smaller scales,  $\zeta$  would then scale as  $\mathcal{O}(h^{-1.55})$ . If the vortices stretch within the updraft, their cross-sections decrease and their vorticity increases, causing the slope of the vorticity line to decrease. Under this scenario,  $-1.55$  would provide an upper bound for the vorticity line slope of a tornado forming by vortex sheet roll-up. That tornadoes may derive much of their energy from vortex sheet vortices is made plausible by the fact that energy can cascade from smaller to larger scales in two-dimensional flows (Chorin 1994). Vortex sheet vortices and tornadoes (at least near the surface) are approximately two-dimensional.

## 5. Vortex gases

In this section we give an overview of a vortex gas theory for two dimensions and a vortex gas model for three dimensions. We introduce a notion of entropy and temperature that is different from the usual notions of entropy and temperature of gases of molecules. We use the theory and models described here to address the question of tornadogenesis and maintenance. The interaction of large numbers of vortices in two- and three-dimensional space

has been studied by modeling the vortices as part of a vortex gas. This theory has its origins in the 19th century in the works of (Helmholtz 1858) and (Thomson 1869). The theory is the analogue of the classical statistical mechanics of gases, which attempts to explain the macroscopic behavior of gases by using the statistics of modeled microscopic behavior of molecules. In the vortex gas case the molecules are replaced by vortices. These could also be arching vortex lines (tubes). Just as in the case of gases, our development includes specialized entropy and temperature. Onsager first suggested the notion of temperature for vortex gases and formulated a two-dimensional theory (Onsager 1949). For a discussion of these ideas see (Chorin 1994, 1993). We follow the development of (Chorin 1994; Chorin and Marsden 1993; Newton 2001), being guided by the work and energy balance analysis of (Lilly 1986a) and finding some analogues in turbulence theory that one could apply to the development of rotation in tornadoes. In classical thermodynamics a body in contact with a heat bath will heat up until it achieves equilibrium with its environment. By analogy, a vortex will heat up if it interacts with “hotter” vortices. As this process repeats itself many times, the vortex eventually achieves quasi-equilibrium with its environment. These “hot” vortices will have negative temperature (in the sense of vortex gas theory) and will increase the energy of a developing vortex. In the case where the vortex is a tornado or pre-tornado, this gives us a mechanism for understanding some aspects of tornadogenesis and maintenance. A critique of the notion of negative temperature in

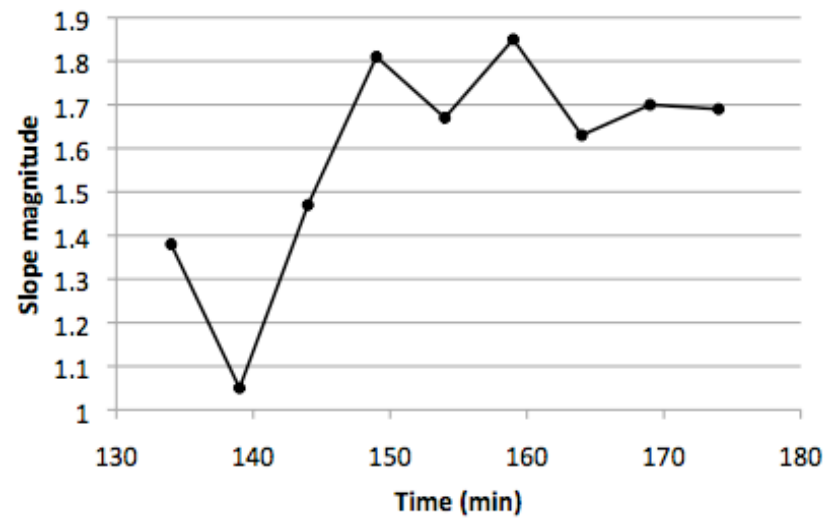
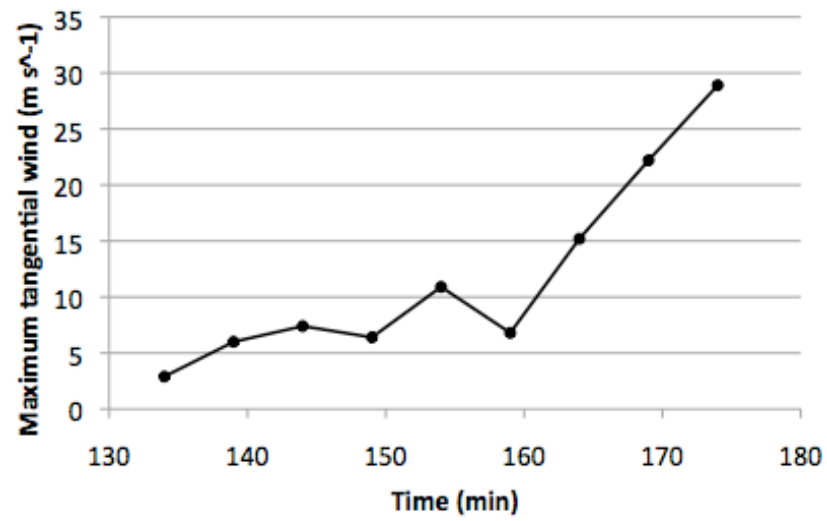
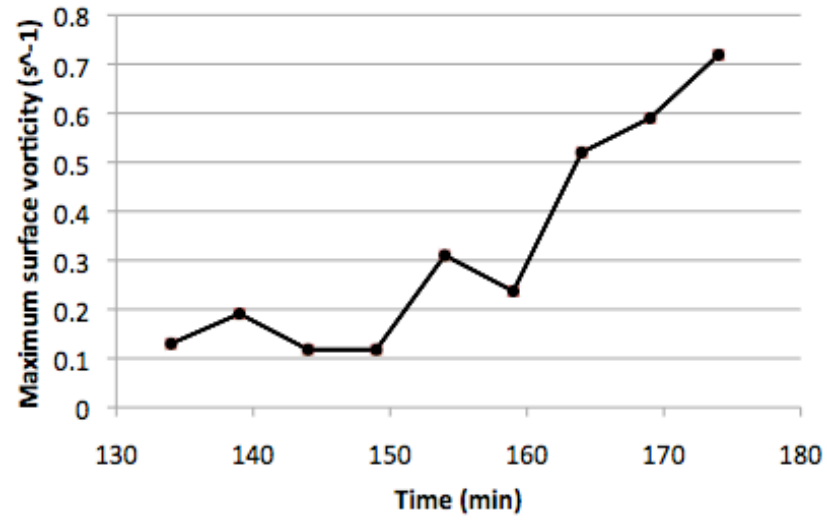


Figure 8: Time series of (a) maximum surface vorticity ( $s^{-1}$ ), (b)  $V_T$  ( $m s^{-1}$ ), and (c) vorticity line slope magnitude.

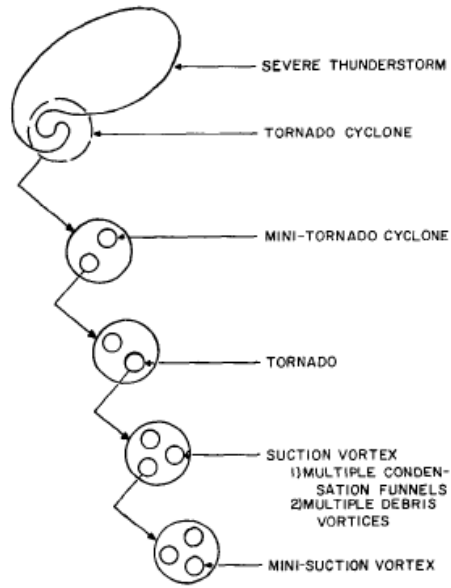


Figure 9: ©American Meteorological Society, Tornado Vortex Simulation at Purdue University. *BAMS*, **58**, 900–908.

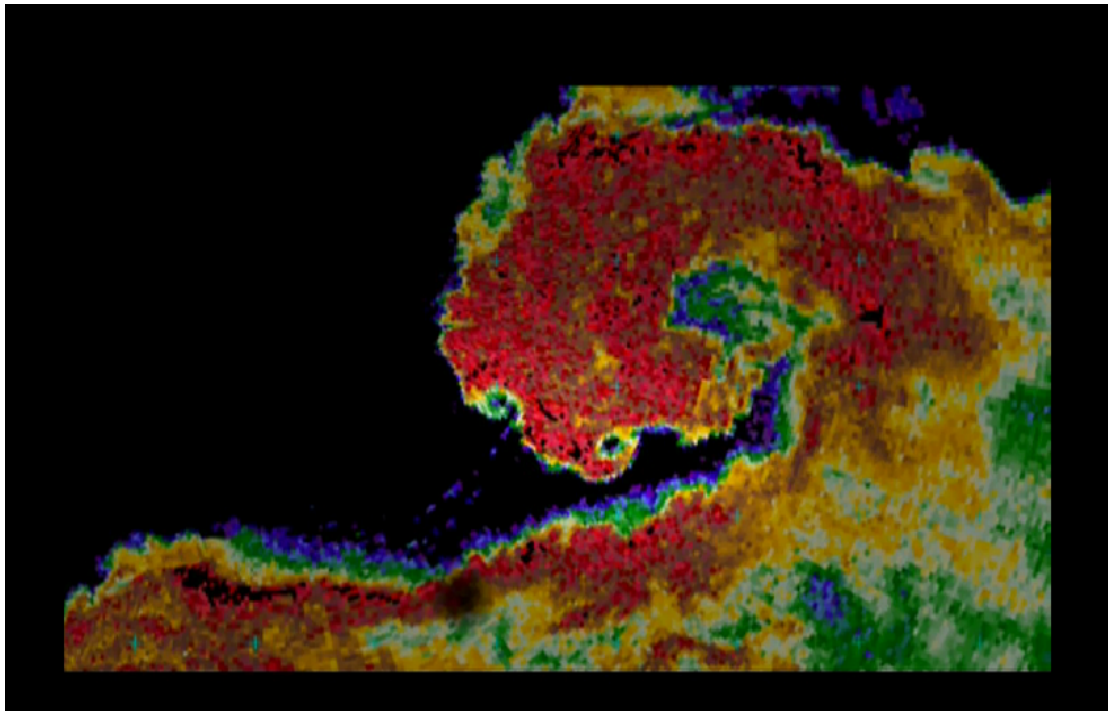


Figure 10: ©Joshua Wurman

the two-dimensional vortex gas theory has been given by Fröhlich and Ruelle (Fröhlich and Ruelle 1982) and Miller (Miller et al. 1992).

The modeling of vortices in three dimensions has been carried out using the Ising model (Chorin and Akao 1991). It uses this simplified approach to the vortex gas to study the relationship of stretching and temperature of the vortex and other quantities associated to a vortex gas. In this approach the vortices appear as either horizontal or vertical segments joining adjacent points in a three-dimensional lattice. The lattice is formed from the points in the three-dimensional space with integer coordinates,  $\mathbb{Z}^3$ . As time advances, the vortex configuration is allowed to change with certain restrictions; specifically, vortices are not allowed to self-intersect. The future configurations of the vortices are then studied using a Monte Carlo Markov chain algorithm.

In the last part of this section we take into account the cross-sections of vortices by using the Kelvin circulation theorem to combine the results of (Cai 2005; Wurman and Gill 2000; Wurman and Alexander 2005) with an argument of (Chorin 1994) and use it to obtain information on the possible source of increase in vorticity at tornado scales.

#### a. The two-dimensional vortex gas theory

The Euler equation for incompressible fluid flow is a limit of the vortex gas equation:

$$\frac{D\mathbf{V}}{Dt} = \frac{\partial\mathbf{V}}{\partial t} + (\mathbf{V} \cdot \nabla)\mathbf{V} = -\nabla p + \mathbf{f},$$

where  $\mathbf{V}$  is the velocity,  $p$  is the pressure, and  $\mathbf{f}$  an external body force. To obtain the equation for vorticity,  $\boldsymbol{\omega} = \text{curl } \mathbf{V} = \nabla \times \mathbf{V}$ , we take the curl of the above equation and obtain

$$\frac{D\boldsymbol{\omega}}{Dt} = (\boldsymbol{\omega} \cdot \nabla)\mathbf{V}.$$

It is possible to extract the  $z$  (vertical) component of vorticity,  $\zeta$ , from the above equation to obtain (Klemp 1987)

$$\frac{\partial\zeta}{\partial t} = -\mathbf{V} \cdot \nabla\zeta + \zeta \frac{\partial w}{\partial z} + \boldsymbol{\omega}_H \cdot \nabla_H w,$$

where  $w$  is the vertical component of the velocity,  $\boldsymbol{\omega}_H$  is the horizontal component of the vorticity, and  $\nabla_H$  is the horizontal gradient. The three terms on the right-hand side of the above equation represent the change in vertical vorticity due to the advection, stretching and tilting of vorticity, respectively.

Vortices that form in strongly sheared environments have a two-dimensional structure before they are stretched. Recently, (Nolan 2012) has shown that a significant amount of the perturbation energy in tornadoes is due to stretching by the updraft near the surface. To model the flow behavior of an intense vortex at the surface, we assume the flow

is essentially two dimensional, although this does not fully capture three-dimensional behavior of the vortex. Under the influence of strong rotation, turbulent flow becomes anisotropic and the flow tends to become two-dimensional but never quite reaches that state (Pouquet and Mininni 2010). Comparing the tracks left by suction spots in tornadoes (Figure 2) and plots of interacting two-dimensional vortices (Figure 11) suggests that there is a connection between the two. The tracks suggest that the vortices behave like two-dimensional vortices, then dissipate due to stretching. This phenomenon can be observed in videos of intense tornadoes.

We proceed to develop the two-dimensional theory to model the two-dimensional behavior. We then develop the three-dimensional model to more fully understand dissipation. The two-dimensional vorticity equation for incompressible fluid flow is

$$\frac{D\boldsymbol{\omega}}{Dt} = 0.$$

Writing the velocity in the component form,  $\mathbf{V} = (u, v)$ , the incompressibility condition,  $\text{div } \mathbf{V} = 0$ , together with the assumption that the underlying domain is simply connected (has no holes) implies that there exists a stream function,  $\psi(x, y)$ , such that

$$u = \frac{\partial\psi}{\partial y}, \quad v = -\frac{\partial\psi}{\partial x} \quad (5.1)$$

and

$$-\Delta\psi = \zeta. \quad (5.2)$$

Assume that vorticity is concentrated at discrete points  $\mathbf{x}_i = (x_i, y_i)$  for  $i = 1, \dots, n$ , each with circulation  $\Gamma_i$ , so that

$$\zeta(\mathbf{x}) = \sum_{i=1}^n \Gamma_i \delta(\mathbf{x} - \mathbf{x}_i),$$

where  $\delta$  denotes the Dirac delta function and  $\mathbf{x} = (x, y)$ . The solution to (5.2) is given by

$$\psi(\mathbf{x}) = -\sum_{i=1}^n \frac{\Gamma_i}{2\pi} \log \|\mathbf{x} - \mathbf{x}_i\|,$$

and, using (5.1), the velocity field induced by the  $j$ th vortex is,

$$V_j(\mathbf{x}) = \frac{\Gamma_j}{2\pi r^2} (y_j - y, -(x_j - x)),$$

where  $r = \|\mathbf{x} - \mathbf{x}_j\|$ .

If one assumes that each of the vortices moves under the influence of the combined velocity field of the remaining vortices, then

$$\frac{d\mathbf{x}_i}{dt} = \sum_{\substack{j=1 \\ j \neq i}}^n V_j(\mathbf{x}_i) = \sum_{j \neq i}^n V_j(\mathbf{x}_i),$$

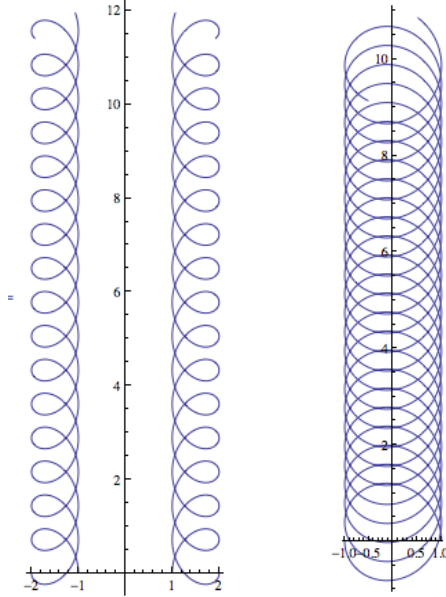


Figure 11: Graphs of interacting point vortices have tracks similar to suction vortex tracks.

or, in the component form,

$$\begin{aligned}\frac{dx_i}{dt} &= \frac{1}{2\pi} \sum_{j \neq i} \frac{\Gamma_j (y_j - y_i)}{r_{ij}^2} \\ \frac{dy_i}{dt} &= -\frac{1}{2\pi} \sum_{j \neq i} \frac{\Gamma_j (x_j - x_i)}{r_{ij}^2},\end{aligned}$$

where  $r_{ij} = \|\mathbf{x}_i - \mathbf{x}_j\|$ . These equations form a Hamiltonian system that has rigorous connections with the Euler equation (Marchioro and Pulvirenti 1994; Chorin and Marsden 1993). The corresponding Hamiltonian is

$$H = -\frac{1}{4\pi} \sum_{\substack{1 \leq i, j \leq n \\ i \neq j}} \Gamma_i \Gamma_j \log \|\mathbf{x}_i - \mathbf{x}_j\|.$$

It is easy to check that the Hamiltonian is conserved, i.e.,

$$\frac{dH}{dt} = 0,$$

which, in particular, implies that if all the circulations are of the same sign, then the vortices cannot merge in finite time. Other conserved quantities are the total vorticity,  $\Gamma$ , the center of vorticity,  $\mathbf{M}$ , and the moment of inertia,  $I$ , given by

$$\Gamma = \sum \Gamma_i, \quad \mathbf{M} = \frac{\sum \Gamma_i \mathbf{x}_i}{\Gamma}, \quad I = \sum \Gamma_i \|\mathbf{x}_i - \mathbf{M}\|^2,$$

where all the sums are for  $i = 1, \dots, n$ .

Using this representation, one can model the behavior of vortex configurations in the plane (Lim and Nebus 2007;

Newton 2001; Marchioro and Pulvirenti 1994). For example, a pair of vortices of equal circulations will move about the midpoint of the segment joining them (Lim and Nebus 2007), p. 92. For a line of vortices of equal circulations, the vortices stay in a line (Lim and Nebus 2007), p. 99. If one has a half line of vortices located at integer points on the  $x$ -axis and terminating at a  $x = 0$ , the vortex line rolls up into a spiral (Chorin and Bernard 1973).

We next provide a brief development of a two-dimensional theory of vortex gases by proceeding in analogy with the development of the Boltzmann distribution in the theory of statistical mechanics in three dimensions. The particles are replaced by vortices and the assumptions on the distribution of vortices in a region in two-dimensional space is used to define a distribution in the corresponding phase space. The entropy of the distribution is defined. The discussion that follows is general and can be used in the context of both two- and three-dimensional flows.

Consider a vortex system, with  $k$  possible energy and moments of inertia levels  $(E_j, I_j)$ ,  $j = 1, \dots, k$ . Let  $0 \leq p_j \leq 1$  represent the probabilities that the system is in the energy state  $E_j$  with the moment of inertia  $I_j$ . We assume that the average energy of the ensemble,  $\langle E \rangle$ , and the average moment of inertia,  $\langle I \rangle$ , are fixed. Then

$$\sum_{j=1}^k p_j = 1, \quad (5.3)$$

$$\sum_{j=1}^k p_j E_j = \langle E \rangle, \quad (5.4)$$

$$\sum_{j=1}^k p_j I_j = \langle I \rangle. \quad (5.5)$$

We define the entropy of the ensemble corresponding to the macrostate  $(\langle E \rangle, \langle I \rangle)$ , up to an additive constant, as

$$S = - \sum_{j=1}^k p_j \log p_j. \quad (5.6)$$

To maximize the entropy, we consider the Lagrangian

$$L(p_1, \dots, p_k) = - \sum_{j=1}^k p_j \log p_j - \alpha \left( \sum_{j=1}^k p_j - 1 \right) - \beta \left( \sum_{j=1}^k p_j E_j - \langle E \rangle \right) - \gamma \left( \sum_{j=1}^k p_j I_j - \langle I \rangle \right), \quad (5.7)$$

where  $\alpha$ ,  $\beta$  and  $\gamma$  are Lagrange multipliers. Differentiating (5.7) with respect to each of the  $p_j$  and setting these partial derivatives equal to zero, we obtain

$$- \log p_j - 1 - \alpha - \beta E_j - \gamma I_j = 0, \quad j = 1, \dots, k,$$

while the derivatives with the respect to the Lagrange multipliers return the constraints (5.3)–(5.5). This results in

$$p_j = e^{-1-\alpha-\beta E_j-\gamma I_j}, \quad j = 1, \dots, k. \quad (5.8)$$

From (5.3) and (5.8) we now have

$$e^{1+\alpha} = \sum_{j=1}^k e^{-\beta E_j - \gamma I_j} \equiv Z, \quad (5.9)$$

where  $Z$  is called a partition function. It follows that

$$p_j = \frac{e^{-\beta E_j - \gamma I_j}}{Z},$$

and from (5.4) and (5.5) we have

$$\langle E \rangle = \sum_{j=1}^k E_j \frac{e^{-\beta E_j - \gamma I_j}}{Z}, \quad \langle I \rangle = \sum_{j=1}^k I_j \frac{e^{-\beta E_j - \gamma I_j}}{Z}.$$

Consequently, using the definition of the partition function (5.9), we obtain

$$\begin{aligned} - \frac{\partial \log Z}{\partial \beta} &= \frac{\sum_{j=1}^k E_j e^{-\beta E_j - \gamma I_j}}{Z} = \langle E \rangle, \\ - \frac{\partial \log Z}{\partial \gamma} &= \frac{\sum_{j=1}^k I_j e^{-\beta E_j - \gamma I_j}}{Z} = \langle I \rangle. \end{aligned} \quad (5.10)$$

The expression (5.6) for the entropy can be written as

$$S = \sum_{j=1}^k p_j (\beta E_j + \gamma I_j + \log Z) = \beta \langle E \rangle + \gamma \langle I \rangle + \log Z,$$

and differentiating it with respect to  $\langle E \rangle$  and using (5.10) gives

$$\begin{aligned} \frac{\partial S}{\partial \langle E \rangle} &= \frac{\partial \beta}{\partial \langle E \rangle} \langle E \rangle + \beta + \frac{\partial \gamma}{\partial \langle E \rangle} \langle I \rangle \\ &+ \frac{\partial \log Z}{\partial \beta} \frac{\partial \beta}{\partial \langle E \rangle} + \frac{\partial \log Z}{\partial \gamma} \frac{\partial \gamma}{\partial \langle E \rangle} \\ &= \beta \equiv \frac{1}{T}, \end{aligned} \quad (5.11)$$

where  $T$  is called the temperature associated with the vortex configuration, and  $\beta$  is the corresponding inverse temperature, or “coldness” according to (Garrod 1995). From now on we will use “temperature” in this particular sense. By a similar process, we can also obtain  $\frac{\partial S}{\partial \langle I \rangle} = \gamma$ , etc. in case of more constraints.

### b. Three-dimensional vortex gas model

A model of three-dimensional vortex gases is much more difficult and has been developed only in special cases. Given a vorticity field  $\boldsymbol{\omega}(\mathbf{x})$  in  $\mathbb{R}^3$ , the system

$$\boldsymbol{\omega} = \nabla \times \mathbf{V}, \quad \nabla \cdot \mathbf{V} = 0$$

can be solved for the velocity field  $\mathbf{V}(\mathbf{x})$  under the assumption that  $\boldsymbol{\omega}(\mathbf{x})$  decays sufficiently fast as  $\|\mathbf{x}\| \rightarrow \infty$  (Majda and Bertozzi 2001). For the velocity field we get

$$\mathbf{V}(\mathbf{x}) = - \frac{1}{4\pi} \int \frac{(\mathbf{x} - \mathbf{x}') \times \boldsymbol{\omega}(\mathbf{x}')}{\|\mathbf{x} - \mathbf{x}'\|^3} d\mathbf{x}',$$

and the kinetic energy can be written as

$$E = \frac{1}{8\pi} \iint \frac{\boldsymbol{\omega}(\mathbf{x}) \cdot \boldsymbol{\omega}(\mathbf{x}')}{\|\mathbf{x} - \mathbf{x}'\|} d\mathbf{x}' d\mathbf{x}. \quad (5.12)$$

#### 1) CHORIN'S MONTE CARLO SETUP

Vortex gases in three dimensions have been modeled in (Chorin and Akao 1991; Chorin 1994) assuming that vortices were made up of vertical and horizontal line segments connecting adjacent points on an integer lattice in the three-dimensional space,  $\mathbb{Z}^3$ . The vortices were supported on an oriented, self-avoiding random walk on the lattice. In the model, the expression (5.12) for the kinetic energy of one vortex becomes

$$E = \frac{1}{8\pi} \sum_i \sum_{j \neq i} \frac{\boldsymbol{\omega}_i \cdot \boldsymbol{\omega}_j}{\|i - j\|} + \frac{1}{8\pi} \sum_i E_{ii},$$

where  $i$  and  $j$  are the three-dimensional coordinates of the locations of the centers of the vortex segments making up the vortex,  $E_{ii}$  is the “self-energy” term of the  $i$ th segment that is a constant and is, therefore, neglected,  $\|i - j\|$  is the distance between the  $i$ th and  $j$ th segment, and  $\boldsymbol{\omega}_i$  is the

vorticity of the  $i$ th segment. The velocity field was carefully defined using a cut-off function to prevent singularities and keep the terms in the sum defined. Similar ideas can be also used in the two-dimensional case.

To describe the state of such a vortex from a statistical viewpoint, Chorin (Chorin 1994) defines the probability of a vortex with energy  $E$  and inverse temperature  $\beta$  via  $P(E) = \frac{e^{-\beta E}}{Z}$ , where  $Z$  is a partition function. This probability is then maximized with respect to permissible configurations of the vortex for various fixed values of  $\beta$  (positive, negative, and zero) using a Metropolis rejection algorithm. Note that from (5.11), as  $\beta$  decreases from  $+\infty$  to 0, and then to  $-\infty$ , the temperature  $T = 1/\beta$  increases from 0 through positive values to  $+\infty = -\infty$  (denoted by  $\infty$  in what follows), and then increases through negative values to  $-0$ .

Chorin studied vortices of various lengths, and concluded that a stretched negative-temperature ( $\beta < 0$ ) vortex must fold assuming energy is conserved. In addition, as vortices with negative temperatures stretch, their temperature decreases to  $T = \infty$  ( $\beta = 0$ ), and they become fractal. Note that as temperature crosses from negative to positive through  $T = \infty$ , the vortices tangle into three-dimensional configurations (Chorin and Akao 1991; Chorin 1994). It is also possible to model a fluid made up of several sparsely distributed vortices, but not without a significant increase in the computational complexity (Marchioro and Pulvirenti 1994). The experimental probabilities of the various configurations of the vortices can be found by performing Markov Chain Monte Carlo simulations (Chorin and Akao 1991).

## 2) ENTROPY AND TEMPERATURE

We can think of entropy of a collection of vortices (vortex gas) as a sum of its configurational entropy and a structural entropy corresponding to stretching, kinking, and collapse of each vortex. Vortices moving into a region where there is a convergent updraft will become more spatially organized (i.e., the configurational entropy decreases; see Figure 1) and will be stretched due to the updraft (i.e., the structural entropy decreases). Since the stretching is accompanied by an increase in energy, we have  $dS/dE = \beta = 1/T < 0$ , so the system's temperature must be negative.

Considering the structural entropy of a vortex and its energy given by (5.12), we can analogously define the temperature of an individual vortex. We now argue that vortices with negative temperature are straight and those with infinite temperature are fractal. Let us assume that  $T < 0$ , so that also  $\beta < 0$ . Since the probability of a configuration of a vortex with energy  $E$  is  $P(E) = e^{-\beta E}/Z$ , the most likely configurations are those with a large positive energy  $E$ .

For a vortex with small cross section and nearly constant cross-sectional vorticity, the energy (5.12) will be maximized if the dot products,  $\boldsymbol{\omega}(\mathbf{x}) \cdot \boldsymbol{\omega}(\mathbf{x}')$ , are as large as possible, hence the vortex should be straight. These comments can be generalized to a configuration with more than one vortex in which case they would be nearly parallel. Therefore, the highest-temperature (hottest) vortices (negative temperatures near  $-0$ ) are the straightest. On the other hand, as  $\beta = 1/T$  approaches  $-0$  (i.e.,  $T$  approaches  $-\infty$ ), the probability distribution becomes uniform. In that case, all the orientations are equally likely, and the vortex configuration can be fractal. Hence, as negative-temperature vortices are stretched, they cool down and kink up as they dissipate.

Next we show, following (Chorin 1994), that if  $T_1$  is the temperature of a vortex with energy  $E_1$ , and  $T_2$  is the temperature of a vortex with energy  $E_2$ , and the vortex systems are combined, then, assuming conservation of energy, three cases are possible:

- i. If  $T_2 > T_1 > 0$ , then  $\frac{d\langle E_2 \rangle}{dt} < 0$  and  $\frac{d\langle E_1 \rangle}{dt} > 0$ ;
- ii. If  $T_1 > 0 > T_2$ , then  $\frac{d\langle E_2 \rangle}{dt} < 0$  and  $\frac{d\langle E_1 \rangle}{dt} > 0$ ;
- iii. If  $0 > T_2 > T_1$ , then  $\frac{d\langle E_2 \rangle}{dt} < 0$  and  $\frac{d\langle E_1 \rangle}{dt} > 0$ .

Hence, for a vortex with a negative temperature, the closer the temperature is to 0, the ‘‘hotter’’ the vortex is. If two vortices interact as a combined system, in which the hotter vortex will lose energy to the lower temperature vortex, the system moves to an equilibrium state.

To show the three claims above, consider two vortices, one with energy  $E_1$  and a developing tornado with energy  $E_2$ . We may regard this as two disjoint vortex systems, each separately in equilibrium. Assume the vortex with energy  $E_1$  moves into a developing tornado with energy  $E_2$  and that their probability densities are independent. Then the energy,  $\langle E \rangle$ , and the entropy,  $\langle S \rangle$ , of the combined vortex system are

$$\langle E \rangle = \langle E_1 \rangle + \langle E_2 \rangle \quad \text{and} \quad S = S_1 + S_2.$$

As the combined vortex system adjusts to equilibrium, the time rate of change of the total entropy satisfies

$$\frac{dS}{dt} = \frac{dS_1}{dt} + \frac{dS_2}{dt} = \frac{dS_1}{d\langle E_1 \rangle} \frac{d\langle E_1 \rangle}{dt} + \frac{dS_2}{d\langle E_2 \rangle} \frac{d\langle E_2 \rangle}{dt} > 0.$$

Conservation of energy implies that

$$\frac{d\langle E \rangle}{dt} = \frac{d\langle E_1 \rangle}{dt} + \frac{d\langle E_2 \rangle}{dt} = 0.$$

Hence,

$$\frac{dS}{dt} = \left( \frac{dS_1}{d\langle E_1 \rangle} - \frac{dS_2}{d\langle E_2 \rangle} \right) \frac{d\langle E_1 \rangle}{dt} = \left( \frac{1}{T_1} - \frac{1}{T_2} \right) \frac{d\langle E_1 \rangle}{dt} > 0,$$

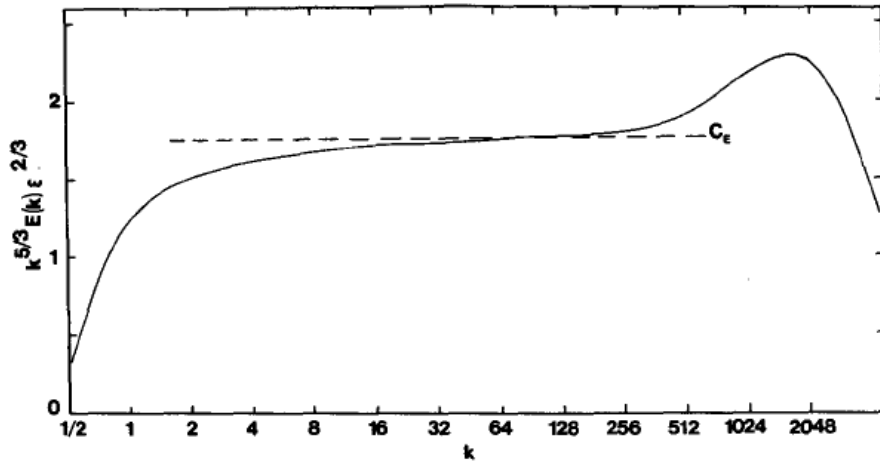


FIG. 13. Inertially weighted energy spectrum,  $k^{5/3}E(k, t)\epsilon^{-2/3}$ , corresponding to the  $t = 8$  curve on Fig. 12. (From André and LeSieur, 1977.)

Figure 12: Inertially weighted energy spectrum corresponding to time  $t = 8$ , for a turbulent flow with low helicity showing high dissipation at large scales (small  $k$ ). ©American Meteorological Society

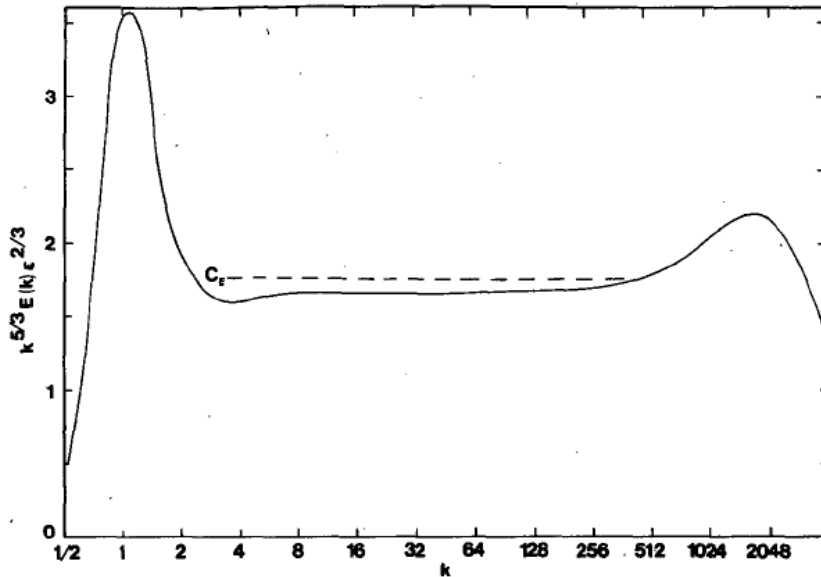


FIG. 15. Inertially weighted spectrum correspondence to the  $t = 12$  curve of Fig. 14. (From André and LeSieur, 1977.)

Figure 13: Inertially weighted energy spectrum corresponding to time  $t = 12$ , for a turbulent flow with high helicity showing low dissipation at large scales (small  $k$ ). ©American Meteorological Society



and the three cases i–iii above follow.

Therefore, negative temperatures are “warmer” than positive temperatures, and negative temperatures that are closer to zero are warmer than negative temperatures that are farther from zero. Hence, as hot, negative-temperature vortices move into the developing tornado, they stretch and cool down, and the ambient vortex heats up. As this process repeats itself many times, the tornado vortex achieves a quasi-equilibrium with the environment.

Generalizing Chorin’s argument used in the two-dimensional model (Chorin 1994), we consider a three-dimensional system in equilibrium, partition the system into boxes, and assume that the vortices are sparsely located, one per box, and nearly parallel and vertical. Let  $E_{tot} = \frac{1}{2} \sum_i m_i U_i^2 + \sum_i E_i$ , where  $m_i$  is the mass of the  $i$ th box in the partition, and  $U_i$  and  $E_i$  are the velocity and potential energy of the vortex in the  $i$ th box, respectively. If  $T_i < 0$ , then  $dS_i/d\langle E_i \rangle < 0$ , and hence, as the entropy increases, the energy is transferred from  $E_i$  to  $U_i$ . This explains the increase in the vorticity of the tornado as hot (negative-temperature) vortices enter the tornado. The vortices entering the tornado are stretched and begin to cool down and they kink up. As this happens, the entropy increases ( $\Delta S > 0$ ) and energy of the vortex decreases ( $\Delta \langle E \rangle < 0$ ) as it is transferred to the larger-scale flow, increasing the kinetic energy. This is the opposite of the situation considered above, where  $\Delta S < 0$  and  $\Delta \langle E \rangle > 0$ , but  $\beta = dS/d\langle E \rangle < 0$ .

We can illustrate a train of vortices in a vortex sheet entering the tornado and transferring the energy to the large scale by replacing the stretching term in the vertical vorticity evolution equation

$$\frac{\partial \zeta}{\partial t} \approx \zeta \frac{\partial w}{\partial z}$$

with a train of delta functions in the form

$$\frac{\partial \zeta}{\partial t} = \sum \Gamma_i \delta_i = \sum \Gamma_i \delta(t - iT),$$

where  $T$  is the time interval between successive vortices entering the tornado. The response of the vertical vorticity to this forcing is a step function with jumps of the size  $\Gamma_i$ .

### c. Energy Spectrum and Power Laws of Cai and Wurman

Chorin (Chorin 1994) gives two possible power laws of dissipation of energy with scale:  $\langle E \rangle(k) \sim k^{-5/3}$  and  $\langle E \rangle(k) \sim k^{-2}$ , where  $k$  is the wave number. The former law is derived by a scaling argument due to Kolmogorov and is also supported by his filament model using results from a Monte Carlo simulation. The latter law is derived as an alternative and is based on a possible form of the energy cascade. (Chorin 1994) also claims that the latter one is a “better candidate for the mean field result.”

The filament model can be applied to analyze a vortex tube in a homogeneous sparse suspension of tubes (Chorin 1994). We define the integral

$$S_r = \left\langle \int_{|\mathbf{r}| \leq r} \boldsymbol{\omega}(\mathbf{x}) \cdot \boldsymbol{\omega}(\mathbf{x} + \mathbf{r}) d\mathbf{r} \right\rangle,$$

where the average is taken over all  $\mathbf{x}$  in the vortex tube. Let  $r > 0$  be small enough so that there are no points that belong to other vortex tubes inside the ball  $B_r(\mathbf{x}) = \{\mathbf{x}' : |\mathbf{x}' - \mathbf{x}| < r\}$ . Let  $C_r$  be the part of the center line of the vortex tube inside the ball  $B_r(\mathbf{x})$ .

Assume the vortex tube is small enough so that perpendicular cross sections to the center line of the vortex tube do not intersect. Let  $\Sigma(s)$  be the cross-section of the tube inside  $B_r(\mathbf{x})$  at an “oriented” distance  $s$  from  $\mathbf{x}$ . Then, using disintegration of measure (see (Schwartz 1976)), we have

$$S_r = \left\langle \boldsymbol{\omega}(\mathbf{x}) \cdot \int_{C_r} ds \int_{\Sigma(s)} \boldsymbol{\omega}(\mathbf{x} + \mathbf{r}) d\Sigma(s) \right\rangle.$$

If  $|\Sigma|(s)$  is the Hausdorff measure of  $\Sigma(s)$ , and  $\boldsymbol{\omega}(\mathbf{x} + \mathbf{r})$  is uniform throughout the cross-section  $\Sigma(s)$ , then

$$S_r = \left\langle \boldsymbol{\omega}(\mathbf{x}) \cdot \int_{C_r} |\Sigma|(s) \boldsymbol{\omega}(\mathbf{x} + \mathbf{r}) ds \right\rangle,$$

where  $\mathbf{x} + \mathbf{r} \in C_r$ . Hence,

$$\overline{|\Sigma|} S_N = \overline{|\Sigma|} \langle \sum_{|I-J| \leq r_N} \boldsymbol{\omega}_I \cdot \boldsymbol{\omega}_J \rangle \approx S_r,$$

where  $\overline{|\Sigma|}$  is the “effective” average cross-sectional area of the vortex tube inside  $B_r(\mathbf{x})$ . To obtain the vorticity spectrum  $Z(k)$ , we integrate the Fourier transform of  $S_r$  over a sphere of radius  $k = |\mathbf{k}|$ . This gives  $Z(k) = \mathcal{O}(k^{-\dim \overline{\Sigma} + 1})$ , and, consequently, the energy spectrum satisfies  $E(k) = Z(k)/k^2 = \mathcal{O}(k^{-\dim \overline{\Sigma} - 1})$ , where  $\overline{\Sigma}$  is the characteristic dimension of the cross-sectional area of the vortex tube.

Combining the results in (Cai 2005) with the Kelvin circulation theorem, we can obtain an estimate of the dimension of the cross-sectional area of the vortex. Suppose that  $D_c$  is the dimension of the center line (axis of the vortex) and suppose that  $D$  is the dimension of the support of the vorticity in the vortex filament. Using Chorin’s estimates for the dimensions  $D_c$  of the vortices depending on the sign of their temperature one concludes that for  $T < 0$  the axis of the vortex has the dimension  $D_c = 1$ . From Wurman’s results (Wurman 2002) we suggest that subvortices moving in tornadoes have negative temperature and that their the horizontal cross-sections are fractal. Now we use the additive properties of the Hausdorff measure (Pesin and Climenhaga 2009) to replace  $D - D_c$  by the negative power in Cai’s power law for vorticity. That, in turn, implies that, for  $T < 0$ ,  $E(k)$  has the form  $E(k) \sim k^{-\gamma}$ , where

$2 \leq \gamma$ . In the case  $T > 0$ , we have  $D_c = 3$  according to (Chorin 1994). That gives  $\gamma = 0$ . From conservation of energy, the energy lost in the vortex filament (subvortex), as the temperature of the filament goes from  $T < 0$  to  $T > 0$ , is consistent with the increase in kinetic energy of the surrounding flow. We believe this interpretation is consistent with the tornadogenesis scenarios in earlier parts of the paper.

Writing the Navier–Stokes equation in energy form and taking the Fourier transform, (Chorin 1994) obtains

$$\partial_t E(k) + 2k^2 R^{-1} E(k) = Q(k),$$

where  $Q(k)$  is cubic in  $\hat{\mathbf{u}}(k)$  and comes from the nonlinear term in the Navier–Stokes Equation. This term represents the transfer of energy between wave numbers and has been studied extensively for the case of homogeneous turbulence (Waleffe 1992). Assuming a form of the energy  $E(k) \sim k^{-\gamma}$ , we see that for large scales (small  $k$ ) an increase of the  $E(k)$  corresponds to an increase in  $\gamma$ , which corresponds to a decrease in the power in Cai’s power law. Certain terms have been singled out and studied in relation to inverse cascades of energy. These interactions involve three wave numbers. It was found that the net effect of the so-called nonlocal interactions is to transfer energy from intermediate scales to larger scales. These interactions occur between modes with helicity of the same sign. Lilly (Lilly 1986a,b) discusses the flows without helicity and dissipation of energy in Figure 12 and flows with helicity and low dissipation of energy in Figure 13. These images in Lilly’s paper (Lilly 1986b) are from the paper by (Andre and Lesieur 1977). The images show that isotropic turbulence with helicity has a “bottleneck” at large scales which inhibits the dissipation of energy. Studies have shown that the presence of helicity and low energy dissipation are unlinked unless the helicity is continuously supplied and/or generated at the energy-containing scales; this is associated with inhomogeneity in the mean field (Lilly 1986a,b; Yokoi and Yoshizawa 1993). Such an inhomogeneity would be supplied by surface friction and the rear flank and forward flank downdrafts and/or their gust fronts. The increase in the exponents for the power laws for the vorticity (Cai 2005) as tornadogenesis approaches and or the tornado strengthens suggests the dimension of the cross-sections of the tornado cyclone increases as well. The increase in the exponents for the power laws for the vorticity (Cai 2005) as tornadogenesis approaches is consistent with the helicity production of the flow at the energy-containing scales. Idealized cross-sections of vortices with high helicity exhibit self-similarity. (Compare Figure 9 and image on page 168 of (Arnold and Khesin 1999).) Thus the tornado develops at a focus scale at which much energy and helicity is transferred to and from other scales. This is consistent with the mean power law and helicity contribution to the flow (Pouquet and Mininni 2010).

## 6. Suction Spots

The two-dimensional point vortex theory developed earlier in Section 5 can be applied to pairs of cyclonically rotating vortices in the half-plane. The paths of the pairs of interacting vortices (Figure 11) form the same type of pattern as the tracks of overlapping suction vortices moving through fields (see Figure 2) as observed by (Fujita 1981) and others from the air (Grazulis 1997). Under the influence of strong rotation, turbulent flow becomes anisotropic with the flow tending toward, but never fully becoming, a two-dimensional flow (Pouquet and Mininni 2010). (Suggesting the two dimensional flow may be an attractor in this situation.) We suggest that the increase in the power in Wurman’s and Cai’s power laws are an indication of the anisotropy of the flow. The paths in Figure 2 can be modeled using the two-dimensional vortex gas theory with translating and interacting point vortices (Figure 11). In the first pair of paths in Figure 11, one can identify the two overlapping paths of cyclonically rotating vortices in the left half-plane and two overlapping paths of counter-rotating, anticyclonic, mirror vortices in the right half-plane as the other ends of the arching vortex lines. The image on the right of Figure 11 shows the paths left by two translating-interacting vortices. Both the first pair of paths and the last path in Figure 11 look similar to paths in Figure 2. The tracks left by the suction vortices (Figure 2) suggest the vortices either originate in the larger tornado vortex or move into the tornado vortex, intensify due to stretching, make a partial revolution, and then dissipate. The periodic entering/appearance of the vortices into the tornado suggests that they occur as a result of the roll-up of a vortex sheet as observed in numerical simulations (e.g., (Rotunno 1984) and Figure 3). These vortices may be extremely intense. Some of these intense vortex paths are from one to two yards in diameter (Figure 2), and some are as narrow as 30 cm in diameter (Fujita 1981). In some cases these intense vortices have pulled cornstalks out of clay soil by their roots. We suggest that these vortices have negative temperature and that, as they dissipate, they transfer energy to the larger vortex. This could manifest itself as a vortex breakdown. Indeed, film and video footage of sub-vortices in tornadoes suggest that they behave like one would expect negative-temperature vortices to behave. For example, in some instances the vortices’ appearance is associated with stretching and with strong convergence. This would suggest that the vortex intensification is related to a decrease in entropy and an increase in energy. Numerical simulations of intense vortices in (Fiedler 1994; Fiedler and Rotunno 1986; Lewellen and Lewellen 2007a,b; Lewellen et al. 2000; Xia et al. 2003) suggest that the maximum wind speeds in intense narrow vortices undergoing vortex breakdown may exceed the speed of sound in the vertical direction.

Mobile Doppler radar observations have been made of cases where the tracks of the vortices that appear to originate in the vortex core make a partial revolution about the ambient tornado vortex and dissipate. This might indicate a Hopf bifurcation of the horizontal component of the flow field, creating a two-cell flow structure: downdraft core and a surrounding updraft. Wurman has studied the flow structure of a number of tornadoes using mobile Doppler radar (Wurman 2002). He has found evidence supporting both the creation of vortices inside the tornado and the creation of vortices outside the tornado resulting in a flow potentially enhancing the tornado’s strength. He has also noted that these secondary vortices have a different velocity and shear profile than the parent tornadoes. The tornadoes appear to have a two-cell structure and a modified Rankine combined profile, with mean azimuthal velocity,  $v$ , depending linearly on radius inside the tornado core,  $v = Cr$ , and a power-law drop-off outside the core,  $v = Cr^{-b}$ , where  $0.5 \leq b \leq 0.6$ . In an extreme case (Wurman 2002) found a power-law drop-off approaching  $v = Cr^{-1}$  on one side of an intense tornado. Such a power law drop off would be consistent with vorticity = 0 outside the tornado core on that side. On the side where the drop off was near  $v = Cr^{-b}$ , where  $0.5 \leq b \leq 0.6$ , this would be consistent with vorticity being advected into the tornado, possibly along a vortex sheet spiraling into the tornado. The secondary vortices appear to be single cell with extreme values of shear and extreme transient updrafts. This is consistent with these vortices having negative temperatures in the vortex gas sense (Chorin 1994; Wurman and Gill 2000).

## 7. Conclusions and Future Work

The results of Section 3, the last part of Section 4 and Section 5 suggest that the increase in strength of a developing tornado occurs as a result of the increase in vorticity due to an inverse cascade of energy from smaller scales. Photographic evidence supporting this is given in the photo of Gene Moore in Figure 1. Numerical models have also supported this as well. The connection between tornadoes and nearly continuously (periodically) produced vortices (vortex lines (tubes)) is that the vortices stir or pump the tornado and increase the vorticity (see section 6.2). How frequently vortex lines are produced, their strength, and the stretching of the vortices determine the eventual strength of the tornado. This can be seen from the point of view of the vortex gas theory (Section 5).

The images in Figures 2 and 11 suggest that a two-dimensional flow is an attractor for the three-dimensional flow in a tornado near the surface. If the initial arrangement of the vortices is linear along the vortex sheet, as the roll-up takes place, the vortices fill out a circle-bounded region. In the linear region one might use a shift on a finite alphabet to study the vortex sheet. The coding of a fractal

into the shift on a finite alphabet is used in the study of fractal dimensions as presented by (Edgar 1992). This is a common way to study dynamical systems.

In the radar reflectivity image of the hook echo region of a supercell thunderstorm shown in Figure 10 (Nova 2004; Chorin 1994; Adlerman and Droegemeier 2002), the hooks on the boundary of the region represent successive vortices in the vortex sheet. One can think of this two-dimensional radar image as a Poincaré section of a supercell dynamical system. One often studies dynamical systems associated with Poincaré sections using discrete dynamical systems. These systems often take the form of shifts on finite alphabets, like, for example, the systems studied in (Edgar 1992). In particular, Edgar discusses the boundary of the Highway dragon fractal, shown in Figure 14, whose fractal dimension is  $\sim 1.52$ . This fractal has a crude resemblance to the radar reflectivity image in Figure 10, and several other “dragon” fractals resemble radar reflectivity images with hook echo regions. Interestingly, their fractal dimensions are in the range of the exponents in the power laws discussed in this work (e.g.,  $\sim 1.52$  for the “twindragon” or  $\sim 1.62$  for the “golden dragon”).

We recommend further exploration of the relationships between helicity, temperature (in the vortex gas sense), self-similarity, and the power laws proposed by Cai. The resulting improvements in our understanding of helical atmospheric vortices could improve operational tornadic prediction. To the degree that the vorticity power law extends from observable to tornadic scales, it may also be possible to improve tornado detection and perhaps even estimate maximum tangential winds in tornadoes, as discussed in Cai (2005). These hypotheses should be tested using real radar observations of tornadic and nontornadic supercells.

### *Acknowledgments.*

The four authors, Bělík, Dokken, Scholz, and Shvartsman were supported by National Science Foundation grant DMS-0802959.

## REFERENCES

- Adlerman, E. J. and K. Droegemeier, 2000: A numerical simulation of cyclic tornadogenesis. *20th Conference on Severe Local Storms*, American Meteorological Society, Orlando, FL, 591.
- Adlerman, E. J. and K. Droegemeier, 2002: The sensitivity of numerically simulated cyclic mesocyclogenesis to variations in environmental parameters. *21th Conference on Severe Local Storms*, American Meteorological Society, San Antonio, TX.

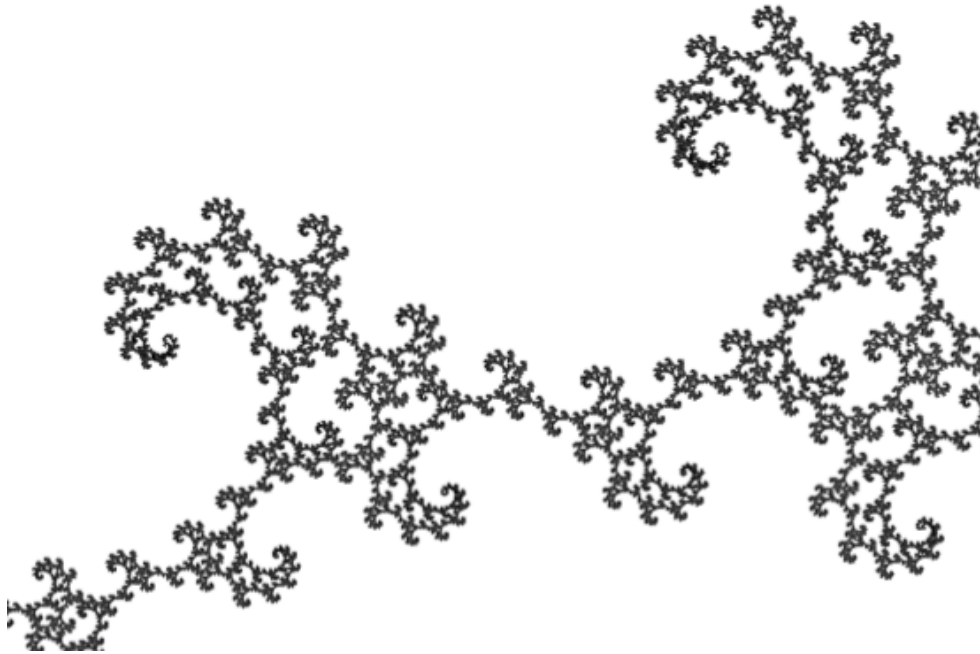


Figure 14: ©Wikipedia Golden Dragon Fractal

- Andre, J. C. and M. Lesieur, 1977: Influence of helicity on the evolution of isotropic turbulence at high Reynolds number. *J. Fluid Mech.*, **81** (1), 187–207.
- Arnold, V. I. and B. A. Khesin, 1999: *Topological Methods in Hydrodynamics*, Applied Mathematical Sciences, Vol. 125. 2d ed., Springer–Verlag, New York.
- Baker, G. R. and M. J. Shelley, 1990: On the connection between thin vortex layers and vortex sheet. *J. Fluid Mech.*, **215**, 161–194.
- Barenblatt, G. I., 1996: *Scaling, self-similarity, and intermediate asymptotics*. Cambridge University Press.
- Barenblatt, G. I., 2003: *Scaling*. Cambridge University Press.
- Barnsley, M., 1988: *Fractals Everywhere*. Academic Press.
- Bluestein, H. B., S. G. Gaddy, D. C. Dowell, A. L. Pazmany, J. C. Galloway, R. E. McIntosh, and H. Stein, 2000: Doppler radar observations of substorm-scale vortices in a supercell. *Monthly Weather Review*, **125**, 1046–1059.
- Bluestein, H. B., W. C. Lee, M. Bell, C. C. Weiss, and A. L. Pazmany, 2003a: Mobile Doppler radar observations of a tornado in a supercell near Bassett, Nebraska, on 5 June 1999. Part II: Tornado-vortex. *Mon. Wea. Rev.*, **131**, 2968–2984.
- Bluestein, H. B. and A. L. Pazmany, 2000: Observations of tornadoes and other convective phenomena with a mobile, 3-mm wavelength, Doppler radar: The spring 1999 field experiment. *Bull. Amer. Met. Soc.*, **81**, 2939–2951.
- Bluestein, H. B., A. L. Pazmany, and C. C. Weiss, 2003b: Mobile Doppler radar observations of a tornado in a supercell near Bassett, Nebraska, on 5 June 1999. Part I: Tornadogenesis. *Mon. Wea. Rev.*, **131**, 2954–2967.
- Brandes, E. A., 1978: Mesocyclone evolution and tornadogenesis: Some observations. *Mon. Wea. Rev.*, **106**, 995–1011.
- Bryan, G. H. and J. M. Fritsch, 2002: A benchmark simulation for moist hydrodynamic numerical models. *Mon. Wea. Rev.*, **130**, 2917–2928.
- Bélik, P., D. P. Dokken, K. Scholz, and M. M. Shvartsman, 2014: Fractal powers in Serrin’s swirling vortex model. *Asymptot. Anal.*, to appear.
- Cai, H., 2005: Comparison between tornadic and nontornadic mesocyclones using the vorticity (pseudovorticity) line technique. *Mon. Wea. Rev.*, **133** (9), 2535–2551.
- Chorin, A. J., 1993: Hairpin removal in vortex interactions II. *J. Comp. Phys.*, **107**, 1–9.
- Chorin, A. J., 1994: *Vorticity and turbulence*. Springer–Verlag, New York.

- Chorin, A. J. and J. Akao, 1991: Vortex equilibria in turbulence and quantum analogues. *Physica D*, **52**, 403–414.
- Chorin, A. J. and P. Bernard, 1973: Discretization of a vortex sheet, with an example of roll-up. *J. Comput. Phys.*, **13**, 423–429.
- Chorin, A. J. and J. E. Marsden, 1993: *A Mathematical Introduction to Fluid Dynamics*. 3d ed., Springer–Verlag.
- Church, C. R., J. T. Snow, and E. M. Agee, 1977: Tornado vortex simulation at Purdue University. *Bull. Amer. Meteor. Soc.*, **58** (9), 900–908.
- Cressman, G. P., 1959: An operational objective in analysis system. *Mon. Wea. Rev.*, **87**, 367–374.
- Davies-Jones, R. P., 1982: A new look at the vorticity equation with application to tornadogenesis. *12th Conference on Severe Local Storms*, San Antonio, TX, Amer. Meteor. Soc., 249–252.
- Davies-Jones, R. P., 1984: Streamwise vorticity: the origin of updraft rotation in supercell storms. *J. Atmos. Sci.*, **41**, 2991–3006.
- Davies-Jones, R. P., 1996: Formulas for the baroclinic and barotropic components of vorticity with application to vortex formation near the ground. *Preprints, Seventh Conf. on Mesoscale Processes, Reading, United Kingdom*, Amer. Meteor. Soc., 14–16.
- Davies-Jones, R. P., 2000: A Lagrangian model for baroclinic genesis of mesoscale vortices. Part I: Theory. *J. Atmos. Sci.*, **57**, 715–736.
- Davies-Jones, R. P., 2006a: Integrals of the vorticity equation. Part I: General three- and two-dimensional flows. *J. Atmos. Sci.*, **63**, 598–610.
- Davies-Jones, R. P., 2006b: Integrals of the vorticity equation. Part II: Special two-dimensional flows. *J. Atmos. Sci.*, **63**, 611–616.
- Davies-Jones, R. P., 2008: Can a descending rain curtain in a supercell instigate tornadogenesis barotropically? *J. Atmos. Sci.*, **65**, 2469–2497.
- Davies-Jones, R. P., D. Burgess, and M. Foster, 1990: Helicity as a tornado forecast parameter. *16th Conference on Severe Local Storms*, 588–592.
- Deardorff, J. W., 1980: Stratocumulus-capped mixed layer derived from a three-dimensional model. *Boundary-Layer Meteorology*, **18**, 495–527.
- Discovery.com/stormchasers, 2010: Violent Minnesota wedge tornado intercept!!! <http://www.youtube.com/watch?v=AvD2nDyXSQo>.
- Dowell, D. C. and H. B. Bluestein, 1997: The Arcadia, Oklahoma storm of 17 May 1981: Analysis of a supercell during tornadogenesis. *Mon. Wea. Rev.*, **125**, 2562–2582.
- Dowell, D. C. and H. B. Bluestein, 2002a: The 8 June 1995 McLean, Texas, storm. Part I: Observations of cyclic tornadogenesis. *Mon. Wea. Rev.*, **125**, 2626–2648.
- Dowell, D. C. and H. B. Bluestein, 2002b: The 8 June 1995 McLean, Texas, storm. Part II: Cyclic tornado formation, maintenance, and dissipation. *Mon. Wea. Rev.*, **130**, 2649–2670.
- Dröegemeier, K. K., S. M. Lazarus, and R. P. Davies-Jones, 1993: The influence of helicity on numerically simulated convective storms. *Mon. Wea. Rev.*, **121**, 2005–2029.
- Edgar, G. A., 1992: *Measure, Topology, and Fractal Geometry*. Springer–Verlag.
- Fiedler, B. H., 1994: The thermodynamic speed limit and its violation in axisymmetric numerical simulations of tornado-like vortices. *Atmos. Ocean*, **32** (2), 335–359.
- Fiedler, B. H. and R. Rotunno, 1986: A theory for the maximum windspeed in tornado-like vortices. *J. Atmos. Sci.*, **43** (21), 2328–2440.
- Fröhlich, J. and D. Ruelle, 1982: Statistical mechanics of vortices in an inviscid two-dimensional fluid. *Commun. Math. Phys.*, **87** (1), 1–36.
- Fujita, T. T., 1973: Proposed mechanism of tornado formation from rotating thunderstorm. *8th Conference on Severe Local Storms*, Denver, CO, Amer. Meteor. Soc., 191–196.
- Fujita, T. T., 1975: New evidence from the April 3–4, 1974 tornadoes. *9th Conference on Severe Local Storms*, Norman, OK, Amer. Meteor. Soc., 248–255.
- Fujita, T. T., 1981: Tornadoes and downbursts in the context of generalized planetary scales. *J. Atmos. Sci.*, **38** (8), 1511–1534.
- Garrod, C., 1995: *Statistical Mechanics and Thermodynamics*. Oxford U. Press.
- Grazulis, T. P., 1997: *Significant Tornadoes Update 1992–1995*. Environmental Films, Copyright January 1997, P.O. Box 302, St. Johnsbury, VT 05819.
- Helmholtz, 1858: Über Integrale der hydrodynamischen Gleichungen welche den Wirbelbewegungen entsprechen. *Crelle*, **55**, 25–55.

- Katok, A. and B. Hasselblatt, 1995: *Introduction to the Modern Theory of Dynamical Systems*, Encyclopedia of Mathematics and its Applications, Vol. 54. Cambridge University Press.
- Klemp, J. B., 1987: Dynamics of tornadic thunderstorms. *Ann. Rev. Fluid Mech.*, **19**, 369–402.
- Krasny, R., 1993: Vortex sheet roll-up. *RIMS Workshop on Unstable and Turbulent Motion of Fluid*, Kyoto, Japan, S. Kida, Ed., World Scientific, 43–49.
- Lee, B. D. and R. B. Wilhelmson, 1997a: The numerical simulation of non-supercell tornadogenesis: Part I: Initiation and evolution of pretornadic mesocyclone circulations along a dry outflow boundary. *J. Atmos. Sci.*, **54**, 32–60.
- Lee, B. D. and R. B. Wilhelmson, 1997b: The numerical simulation of non-supercell tornadogenesis, Part II: Evolution of a family of tornadoes along a weak outflow boundary. *J. Atmos. Sci.*, **54**, 2387–2415.
- Lee, B. D. and R. B. Wilhelmson, 2000: The numerical simulation of non-supercell tornadogenesis, Part III: Parameter tests investigating the role of CAPE, vortex sheet strength and boundary layer vertical shear. *J. Atmos. Sci.*, **57**, 2246–2261.
- Levich, E. and E. Tzvetkov, 1985: Helical inverse cascade in three-dimensional turbulence as a fundamental dominant mechanism in mesoscale atmospheric phenomena. *Physics reports*, **128** (1), 1–37.
- Lewellen, D. C. and W. S. Lewellen, 2007a: Near-surface intensification of tornado vortices. *J. Atmos. Sci.*, **64** (7), 2176–2194.
- Lewellen, D. C. and W. S. Lewellen, 2007b: Near-surface vortex intensification through corner flow collapse. *J. Atmos. Sci.*, **64** (7), 2195–2209.
- Lewellen, D. C., W. S. Lewellen, and J. Xia, 2000: The influence of a local swirl ratio on tornado intensification near the surface. *J. Atmos. Sci.*, **57** (4), 527–544.
- Lilly, D. K., 1983: Dynamics of rotating thunderstorms. *Mesoscale Meteorology—Theories, Observations, and Models*, D. K. Lilly and E. T. Gal-Chen, Eds., D. Reidel, Dordrecht, Vol. 114, 531–544.
- Lilly, D. K., 1986a: The structure, energetics and propagation of rotating convective storms. Part I: Energy exchange with the mean flow. *J. Atmos. Sci.*, **43**, 113–125.
- Lilly, D. K., 1986b: The structure, energetics and propagation of rotating convective storms. Part II: Helicity and storm stabilization. *J. Atmos. Sci.*, **43**, 126–140.
- Lim, C. and J. Nebus, 2007: *Vorticity, Statistical Mechanics, and Monte Carlo Simulation*. Springer–Verlag.
- Majda, A. J. and A. Bertozzi, 2001: *Vorticity and Incompressible Flows*. 1st ed., Cambridge Texts in Applied Mathematics, Cambridge University Press.
- Mandelbrot, B. B., 1983: *The fractal geometry of nature*. W.H. Freeman and Company.
- Marchioro, C. and M. Pulvirenti, 1994: *Mathematical Theory of Incompressible Nonviscous Fluids*, Applied Mathematical Sciences, Vol. 96. Springer–Verlag.
- Markowski, P. A., J. M. Straka, and E. N. Rasmussen, 2002: Direct surface thermodynamic observations within the rear-flank downdrafts of nontornadic and tornadic supercells. *Mon. Wea. Rev.*, **130**, 1692–1721.
- Markowski, P. M., J. M. Straka, and E. N. Rasmussen, 2003: Tornadogenesis resulting from transport of circulation by a downdraft: Idealized numerical simulations. *J. Atmos. Sci.*, **60**, 795–823.
- Markowski, P. M., J. M. Straka, E. N. Rasmussen, R. P. Davies-Jones, Y. Richardson, and J. Trapp, 2008: Vortex lines within low-level mesocyclones obtained from pseudo-dual-Doppler radar observations. *Mon. Wea. Rev.*, **136**, 3513–3535.
- Miller, J., P. B. Weichman, and M. C. Cross, 1992: Statistical mechanics, Euler’s equation, and Jupiter’s Red Spot. *Physical Review A*, **45**, 2328–2359.
- Moffat, H. K., 1969: The degree of knottedness of tangled vortex lines. *J. Fluid Mech.*, **35** (1), 117–129.
- Moffat, H. K. and A. Tsinober, 1992: Helicity in laminar and turbulent flow. *Annu. Rev. Fluid Mech.*, **24**, 281–312.
- Morrison, H., J. A. Curry, and V. I. Khvorostyanov, 2005: A new double-moment microphysics parametrization for application in cloud and climate models. Part I: Description. *J. Atmos. Sci.*, **62**, 1665–1677.
- Newton, P. K., 2001: *The N-vortex problem. Analytical Techniques*. Springer–Verlag, New York.
- Nolan, D. S., 2012: Three-dimensional instabilities in tornado-like vortices with secondary circulations. *J. Fluid Mech.*, **711**, 61–100.
- Nova, 2004: Hunt for the super twister. <http://www.pbs.org/wgbh/nova/earth/hunt-for-the-supertwister.html>.
- Onsager, L., 1949: Statistical hydrodynamics. *Il Nuovo Cimento*, **6**, 279–287.

- Pesin, Y. and V. Climenhaga, 2009: *Lectures on Fractal Geometry and Dynamical Systems*, Student Mathematical Library, Vol. 52. AMS, Providence, RI.
- Potvin, C. K., 2013: A variational method for detecting and characterizing intense vortices in Cartesian wind fields. *Mon. Wea. Rev.*, In Press.
- Pouquet, A. and P. D. Mininni, 2010: The interplay between helicity and rotation in turbulence: implications for scaling laws and small-scale dynamics. *Phil. Trans. R. Soc. A*, **368**, 1635–1662.
- Roberts, R. D. and J. W. Wilson, 1995: The genesis of three nonsupercell tornadoes observed with dual-Doppler radar. *Mon. Wea. Rev.*, **123**, 3408–3436.
- Rotunno, R., 1984: An investigation of a three-dimensional asymmetric vortex. *J. Atmos. Sci.*, **41**, 283–298.
- Schwartz, L., 1976: Lectures on disintegration of measures. *Tata Institute of Fundamental Research*.
- Serrin, J., 1972: The swirling vortex. *Phil. Trans. Roy. Soc. London, Series A, Math & Phys. Sci.*, **271 (1214)**, 325–360.
- Snow, J. T., 1978: On inertial instability as related to the multiple vortex phenomena. *J. Atmos. Sci.*, **35**, 1660–1677.
- Straka, J. M., E. N. Rasmussen, R. P. Davies-Jones, and P. M. Markowski, 2007: An observational and idealized numerical examination of low-level counter-rotating vortices toward the rear flank of supercells. *Electronic J. Severe Storms Meteor.*, **2 (8)**, 1–22.
- Thomson, L. K. W., 1869: On vortex motion. *Trans. Roy. Soc. Edinburgh*, **25**, 217–260.
- Trapp, R. J., 1999: Observations of nontornadic low-level mesocyclones and attendant tornadogenesis failure during VORTEX 94. *Mon. Wea. Rev.*, **124**, 384–407.
- Trevorrow, S. T., R. D. Hildner, G. J. Tripoli, and M. L. Bükler, 2012: Numerical study of low-level vorticity prior to tornadogenesis. *26th Conference on Severe Local Storms*, American Meteorological Society, Nashville, TN, Amer. Meteor. Soc.
- Wakimoto, R. M. and N. T. Atkins, 1996: Observations on the origins of rotation: The Newcastle tornado during VORTEX 94. *Mon. Wea. Rev.*, **124**, 384–407.
- Wakimoto, R. M. and J. W. Wilson, 1989: Non-supercell tornadoes. *Mon. Wea. Rev.*, **117**, 1113–1140.
- Waleffe, F., 1992: The nature of triad interactions in homogeneous turbulence. *Phys. Fluids A*, **4 (2)**, 350–363.
- Wilson, J. W., 1986: Tornadogenesis by nonprecipitation induced wind shear lines. *Mon. Wea. Rev.*, **114**, 270–284.
- Wurman, J., 2002: The multiple-vortex structure of a tornado. *Weather and Forecasting*, **17**, 473–505.
- Wurman, J. and C. R. Alexander, 2005: The 30 May 1998 Spencer, South Dakota, storm. Part II: Comparison of observed damage and radar-derived winds in the tornadoes. *Mon. Wea. Rev.*, **133 (1)**, 97–119.
- Wurman, J. and S. Gill, 2000: Fine-scale radar observations of the Dimmitt, Texas (2 June 1995) tornado. *Mon. Wea. Rev.*, **128**, 2135–2164.
- Wurman, J., K. Kosiba, and P. Robinson, 2013: In situ, doppler radar, and video observations of the interior structure of a tornado and the wind-damage relationship. *BAMS*, **94 (6)**, 835–846.
- Xia, J., D. C. Lewellen, and W. S. Lewellen, 2003: Influence of Mach number on tornado corner flow dynamics. *J. Atmos. Sci.*, **60 (22)**, 2820–2825.
- Yokoi, N. and A. Yoshizawa, 1993: Statistical analysis of the effects of helicity in inhomogeneous turbulence. *Phys. Fluids A*, **5 (2)**, 464–477.